Hypoxic memory of tumor intrinsic type I interferon suppression promotes breast cancer metastasis

Oihana Iriondo[1,2,*#†], Desirea Mecenas[1,2*], Yilin Li[1,2,3*], Christopher R. Chin[4], Amal Thomas[5], Yonatan Amzaleg[1,2,6], Veronica Ortiz[1,2], Matthew MacKay[1], Amber Dickerson[1,2], Grace Lee[1,2], Sevana Harotoonian[1], Bérénice A. Benayoun[2,5,7], Andrew Smith[5], Christopher Mason[4], Evanthia T. Roussos Torres[2,8], Min Yu[1,2#]

[1]Department of Stem Cell Biology and Regenerative Medicine, Keck School of Medicine of the University of Southern California, Los Angeles, CA 90033, USA.

[2]USC Norris Comprehensive Cancer Center, Keck School of Medicine of the University of Southern California, Los Angeles, CA 90033, USA

[3]Key Laboratory of Carcinogenesis and Translational Research (Ministry of Education), Peking University Cancer Hospital and Institute, Beijing, China

[4]Department of Department of Physiology and Biophysics, Weill Cornell Medicine, New York, NY 10021, USA

[5]Department of Molecular and Computational Biology, USC Dana and David Dornsife College of Letters, Arts and Sciences, University of Southern California, Los Angeles, CA 90089, USA

[6]Center for Craniofacial Molecular Biology, Ostrow School of Dentistry of the University of Southern California, Los Angeles, CA 90033, USA.

[7]Leonard Davis School of Gerontology, University of Southern California, Los Angeles, CA 90089, USA

[8]Department of Medicine, Keck School of Medicine of the University of Southern California, Los Angeles, CA 90033, USA.

[*]These authors contributed equally to this work.

[#]Correspondence: minyu@med.usc.edu and oiriondo@cicbiogune.es

[†]Present address: CIC bioGUNE, Bizkaia Technology Park, Derio 48160, Spain

Summary

Hypoxia is a common feature of many solid tumors due to aberrant proliferation and angiogenesis and has been associated with tumor progression and metastasis. Most of the well-known hypoxia effects are mediated through hypoxia-inducible factors (HIFs), but the long-lasting effect of hypoxia beyond the immediate HIF regulation remains less understood. Here we show that hypoxia exerts a prolonged effect through HIF-independent mechanisms to promote metastasis. Using breast cancer patient-derived circulating tumor cell (CTC) lines and common breast cancer cell lines, we found that hypoxia downregulates tumor intrinsic type I interferon (IFN) signaling and its downstream antigen presentation (AP) machinery in luminal breast cancer cells. This effect does not depend on the canonical HIFs but is mediated, at least partially, via forkhead box protein O1 (FOXO1). Moreover, hypoxia induced IFN/AP suppression can last longer than the hypoxic exposure, presenting a "hypoxic memory" phenotype. Hypoxic memory of IFN/AP downregulation is established by specific hypoxic priming, and cells with hypoxic memory have an enhanced ability for tumorigenesis and metastasis. The histone deacetylase inhibitor (HDACi) Entinostat can erase the hypoxic memory and improve the immune clearance of tumor cells when combined with checkpoint immunotherapies in a syngeneic breast cancer mouse model. These results point to a novel mechanism for hypoxia facilitated tumor progression, through a long-lasting memory that provides advantages for CTCs during the metastatic cascade.

Introduction

In solid tumors, rapid cell division and aberrant angiogenesis often lead to oxygen deprivation or hypoxia, which has long been associated with increased malignancy, poor prognosis, and resistance to radio- and chemotherapy(Bertout et al., 2008). Hypoxia influences tumor progression through a variety of mechanisms (reviewed in(Rankin et al., 2016)), including promotion of angiogenesis(Pugh and Ratcliffe, 2003), matrix remodeling(Eisinger-Mathason et al., 2013), enhanced cell motility and cancer stem cell content(Iriondo et al., 2015; Li et al., 2009; Yang et al., 2008), and modification of the premetastatic niche(Erler et al., 2009; Wong et al., 2011). Hypoxia-inducible factors (HIFs) play a central role in many of these processes. HIFs are heterodimers composed of an oxygen labile alpha subunit (HIF1α, HIF2α, or the lesser known HIF3α) and a stable beta subunit (HIF1β, also known as ARNT). Under well oxygenated conditions, HIF1α and HIF2α are hydroxylated in two conserved proline residues by EGLN proteins (also known as prolyl hydroxylases, PHDs), bound by the von Hippel-Lindau (VHL) protein and targeted for proteasomal degradation(Bruick and McKnight, 2001; Huang et al., 1998; Ivan et al., 2001). PHDs belong to the 2-oxoglutarate-dependent dioxygenase (2OGDD) superfamily and use O_2 as a co-substrate. Therefore, when oxygen availability is low HIFα is stabilized, binds to HIF1β and regulates the expression of a myriad of genes involved in proliferation, metabolism, cell motility, apoptosis, etc.(Kaelin and Ratcliffe, 2008; Semenza, 2012a). Several studies have underscored the importance of alternative HIF-independent mechanisms in regulating the cellular response to hypoxia. Besides HIFα, PHDs can hydroxylate non-HIFα substrates in an oxygen dependent manner, regulating their stability or activity(Ivan and Kaelin, 2017). In addition, other enzymes from the 2OGDD superfamily of proteins have

been shown to function as oxygen sensors, including TET DNA demethylases(Thienpont et al., 2016) and several Jumonji (JmjC) histone demethylases (KDMs)(Batie et al., 2019a; Chakraborty et al., 2019). Furthermore, some TET and JmjC-KDMs are transcriptionally regulated by HIF(Choudhry and Harris, 2017), highlighting a complex role for hypoxia in shaping the epigenetic landscape of cells.

Tumor hypoxia has been linked to immunosuppression (Chouaib et al., 2017; Vito et al., 2020). Hypoxic areas in tumors attract M2-like tumor associated macrophages (TAMs)(Movahedi et al., 2010; Van Overmeire et al., 2014), myeloid-derived suppressor cells (MDSCs)(Chiu et al., 2017) and regulatory T cells (Tregs), and show reduced CD8 T cell infiltration(Hatfield et al., 2015). Furthermore, hypoxic microenvironments can lead to diminished T cell performance and survival, mostly due to metabolic alterations driven by hypoxia, such as increases in lactic acid and extracellular adenosine(Chouaib et al., 2017; Fischer et al., 2007). However, the effect of hypoxia on tumor cell intrinsic immune evasive features are less characterized.

A key class of cytokines that play pivotal roles in the immune response against infectious agents and tumors are type I interferons (IFNs)(Snell et al., 2017). Type I IFNs are a family of protein consisting of 13 IFNα subunits, IFNβ, and several poorly defined single gene products(Boukhaled et al., 2021). Expression of type I IFNs is induced by the activation of pattern and danger recognition receptors. Once secreted, IFNs signal through the IFNα/β receptor (IFNAR, composed of subunits IFNAR1 and IFNAR2), which phosphorylates JAK1 and TYK2, resulting in phosphorylation and activation of STAT1/STAT2 heterodimers.

Phosphorylated STAT1/STAT2 bind to IRF9 to form the interferon-stimulated gene factor 3 (ISGF3). ISGF3 translocates to the nucleus and binds to interferon signaling response elements (ISRE) to induce the expression of interferon stimulated genes (ISGs). In addition to this canonical signaling, type I IFNs can activate signaling by STAT3-6, JNK, ERK, MAPK and mTOR pathways(Boukhaled et al., 2021). Type I IFNs can regulate tumor growth directly – by impacting cell proliferation and survival – or indirectly – by modulating antitumor immunity or influencing tumor angiogenesis(Parker et al., 2016).

Our previous work has shown that the hypoxia signaling pathway is significantly upregulated in CTCs isolated from patient blood during disease progression compared to those isolated during treatment response(Yu et al., 2013). Hypoxia is a condition that facilitates the establishment of CTC lines(Yu et al., 2013, 2014) with the capacity to metastasize to the major organs of experimental mice, as seen in the corresponding patients(Klotz et al., 2020). Furthermore, recent reports indicate hypoxia in promoting CTC generation and behavior(Donato et al., 2020; Godet et al., 2019). These observations suggest that hypoxia induced molecular changes could play important roles in promoting metastasis.

Results

Hypoxia downregulates IFN and AP pathways in luminal breast cancer cells.

To test if hypoxic cultures impact the tumor formation and metastatic capacity of CTC lines, we grew GFP-LUC labeled CTCs for 8 weeks in normoxic or hypoxic cultures, and then injected them into the mammary fat pads or the tail veins of NSG mice (Figure 1A). Once the CTC lines are established, normoxic culture does not decrease cell growth (Figure S1A) nor significantly

affect cell death (Figure S1B). *In vivo*, BRx50 and BRx68 CTC lines formed larger tumors after being cultured in hypoxia compared to normoxia, while BRx07, BRx42 and BRx61 cells formed similarly sized tumors following culture in both conditions (Figures 1B and S1C). In the setting of experimental metastasis via tail vein injection, 7 out of 10 mice injected with BRx68 cells grown in hypoxic conditions showed metastatic signals detected by bioluminescent imaging 14 weeks after injection, compared to only 1 out of 7 mice injected with BRx68 cells grown in normoxia (Figures 1C and S1D). In contrast, mice injected with BRx07 cells cultured in normoxia or hypoxia showed similar levels of metastasis (Figure S1E).

RNA-seq analysis of BRx68 cells cultured in normoxia or hypoxia for 8 weeks showed 84 genes upregulated and 241 genes downregulated in hypoxia (fold change≥1.5, FDR≤0.05) (Figure 2A; Table S1-S2). Pathway analysis of these differentially expressed genes showed an enrichment for immune related pathways, especially interferon (IFN) signaling and the antigen presentation (AP) pathway. All genes in these pathways showed lower expression in hypoxia (Figure 2B). Similarly, Gene Set Enrichment Analysis (GSEA) with genes downregulated in hypoxia showed significant overlaps with several gene sets involved in interferon response (Table S3). As expected, the list of genes upregulated in hypoxia significantly overlapped with several hypoxia gene sets (Table S4). qPCR analysis confirmed the lower expression of the IFN target genes ISG15, IFIT1 and IFIT3 in BRx68 cells grown in hypoxia and showed similar results with BRx07 and BRx50 cells (Figure 2C). Flow cytometry analysis of the MHC-I molecules in BRx68 and BRx50 also showed significantly reduced levels in cells cultured in hypoxia, compared to those cultured in normoxia for 8 weeks (Figure 2D).

We next set out to determine whether hypoxia reduces the expression of IFN target genes in other breast cancer cell lines. In response to hypoxia, all human cell lines tested upregulated the HIF target genes CA9 and PHD3 (Figure 2E). However, hypoxia reduced IFIT1 and ISG15 expression in MCF7, T47D and BT474 cells, while failing to do so in MDA-MB-231 and HS578T cells (Figure 2E). We also tested mouse mammary tumor cell lines in hypoxia, and found reduced Ifit1 and Isg15 expression levels in Py117(Aguilera et al., 2016) and NT2.5(Song et al., 2008) cells, but not in Py8119(Aguilera et al., 2016) cells (Figure 2F). To investigate the molecular characteristics distinguishing cells that decrease IFN target gene expression in hypoxia (responders) from those that do not (non-responders), we analyzed publicly available RNA-seq datasets of human breast cancer cell lines and microarray data from mouse cell lines. Genes differentially upregulated in responders showed significant overlap with several sets of genes upregulated in luminal tumors (compared to basal tumors) and genes downregulated during epithelial to mesenchymal transition (EMT) (Tables S5). In contrast, genes overexpressed in non-responders overlapped significantly with sets of genes downregulated in luminal tumors and genes upregulated during EMT (Tables S6).

To evaluate whether the same patterns also presented *in vivo*, we next investigated whether tumors from breast cancer patients showed inverse correlations between a hypoxia signature(Buffa et al., 2010) and a signature composed of genes from the IFN and AP pathways that were differentially expressed in our RNA-seq analysis (IFN/AP signature) (Figure 2A; Table S7). Most breast tumors in the TCGA dataset had low scores for both signatures. However, tumors with high scores for the hypoxia signature generally showed low scores for the IFN/AP signature, and vice-versa (Figures 3A and S2A). Since TCGA datasets are obtained from bulk

tumors, the inverse correlation between hypoxia and IFN/AP signatures could be a consequence of the differential recruitment of immune cells to hypoxic vs. non-hypoxic tumors. To explore possible correlations between these 2 signatures in tumor cells *in vivo*, we performed single-cell RNA sequencing (scRNAseq) analysis of spontaneous breast tumors formed in the FVB-MMTV-PyMT mouse model. Using the same mouse model, another group reported that about 2 percent of tumor tissue dissected from 11-weeks-old mice and 10 percent from 16-weeks-old mice were hypoxic(Kuchnio et al., 2015). Taking this into consideration, tumors from two 12-week-old and two 16-week-old mice were dissociated, and cells were subjected to scRNAseq using the Chromium platform. Using Seurat, we first annotated clusters representing different cell types found in the tumor (Figure S2B), and then projected the hypoxia and IFN/AP signatures on the tumor cells (Figure S2C). For each time point, tumor cells were arranged in deciles according to their IFN/AP scores (Figure 3B). The hypoxia scores for the corresponding tumor cells in each decile showed an inverse correlation with the IFN/AP scores at the earlier time point (12 weeks), but a positive correlation at the later time point (16 weeks) (Figures 3B and S2D). This was consistent with our *in vitro* finding, given reports that the MMTV-PyMT model progresses with a loss of luminal features over time(Lin et al., 2003). We also applied the same analysis to a published scRNAseq dataset that includes several syngeneic tumor models(Yeo et al., 2020), and found that all 4 models showed a clear inverse correlation of hypoxia and IFN/AP signatures in Cd24-sorted tumor cells (Figure 3C).

Hypoxic memory of prolonged suppression of IFN/AP promotes tumor progression.

Intrigued by the differences between BRx07 and BRx68 *in vivo*, we assessed the stability of the hypoxia-induced downregulation of IFN target genes upon reoxygenation. In both BRx07 and

BRx68 cells, 3-day reoxygenation results in complete loss of HIF1α expression and decreases HIF target gene expression to same levels as those found after reoxygenation for 7 days (Figures S3A-F). Interestingly, a 3-day reoxygenation period is sufficient to significantly increase IFIT1 and IFIT3 expression levels in BRx07 cells, but not in BRx68 cells (Figures 4A and S3C, S3F). In fact, the increase in IFN target genes observed in BRx07 cells reoxygenated for 3 days was bigger than the increase in cells reoxygenated for 8 weeks (2.9x vs 1.6x for IFIT1, 4x vs 1.75x for IFIT3) (Figure 4A). In BRx68 and BRx50 cells, the increase in IFN target gene expression was only observed when cells were reoxygenated for 8 weeks (Figures 4A and S3G). Accordingly, tumors formed by BRx68 cells grown in normoxia for 3 days were significantly bigger than those formed by cells grown in normoxia for 8 weeks (Figure 4B). Similar maintenance of suppression was also observed in HLA-ABC levels in BRx68 and BRx50 after reoxygenation for 3 days (Figures 2D and S3H).

We next evaluated if the sustained suppression of IFN targets by hypoxia observed in CTC lines also occurs in other breast cancer cell lines. When MCF7 cells were cultured in 4% or 1% O_2 for 14 days and then reoxygenated for 3 days (see Methods), cells that had been grown in 4% O_2 maintained lower IFN target levels, even though the HIF target PHD3 reached basal expression levels (Figure 4C). In contrast, a shorter exposure in hypoxia for 3 days did not maintain the suppression of the IFN target ISG15 (Figure 4E). Tumor growth in the mammary fat pads of NSG mice showed an association with the prolonged suppression of the IFN target: MCF7 cells grown in hypoxia, especially at 4% oxygen, for 14 days formed bigger tumors than those grown in normoxia (Figure 4D), while MCF7 cells grown in various oxygen conditions for 3 days produced similar sized tumors (Figure 4F).

Taken together, these results suggest that certain breast cancer cells can maintain lower IFN signaling even after they exit hypoxic niches, suggesting the existence of a "hypoxic memory". To elucidate whether such "hypoxic memory" can be found *in vivo*, we designed a 2-plasmid reporter system that enables us to permanently mark cells exposed to hypoxia so that they can be tracked during tumor progression (Figure 5A). Cells that express this 2-plasmid reporter system are initially RFP positive but upon exposure to hypoxia, permanently lose RFP expression due to gene excision and start expressing GFP. FACS analysis of MCF7 cells transduced with the 2-plasmid reporter showed that, while the vast majority of cells remained $RFP^{+}GFP^{-}$ when cultured in normoxic conditions, an average of 56.7% of cells grown in hypoxia (1% O_2) for 3 days were GFP^{+} (Figure 5B-C). When the hypoxia tracing MCF7 (MCF7-HypT) cells were cultured in 3D mixed matrigel/collagen gels, spheres that were originally exclusively RFP^{+} developed GFP^{+} areas as they grew, suggesting the system can detect local hypoxia in spheres (Figure 5C). We next injected MCF7-HypT cells into the mammary fat pads of NSG mice. After 8 weeks, mice were injected with the hypoxia detecting probe pimonidazole(Varia et al., 1998), and tumors and lungs were dissected and fixed 90 minutes later. Immunostaining of tissue sections suggests that cells that have been exposed to hypoxia are more efficient in metastasizing to the lung, since the proportion of GFP^{+} metastatic loci in lungs is significantly higher than the proportion of GFP^{+} cells in primary tumors (Figures 5E and S4A-B). Importantly, immunofluorescence staining also revealed that CRE expression was exclusively detected in pimonidazole-positive areas, while GFP^{+} cells could be detected in non-hypoxic areas, showing that many cells had exited hypoxic niches after converting into GFP-expressing cells (Figure 5F). In fact, staining of whole tumor sections demonstrated that the vast majority of GFP^{+} cells were located in pimonidazole-negative

non-hypoxic regions of the tumor (Figure S4C). Strikingly, $RFP^{-}GFP^{+}$ cells sorted from MCF7-HypT tumors showed lower expression levels of IFN target genes than their $RFP^{+}GFP^{-}$ counterparts, even though the expression of the HIF target genes CA9, PHD3 and NDRG1 was not significantly different (Figures 5G and S4D), suggesting that cells retain a memory of their hypoxic past.

HIF-independent increase of FOXO1 protein level in hypoxia suppresses IFN.

To clarify the mechanism by which hypoxia reduces IFN target gene expression in luminal breast cancer cells, we first evaluated whether there are different levels of mitochondrial double strand RNA (dsRNA), an endogenous IFN stimulus, as recently reported(Arnaiz et al., 2020). Immunofluorescence staining using the J2 antibody, which is commonly used to detect mitochondrial dsRNA, did not detect a significant difference between MCF7 cells cultured in normoxia or in 4% or 1% hypoxia for 3 days (Figure S5A). To test whether there were different responses to the same stimulus, we transfected the MCF7 cells that have been cultured in different oxygen levels for 14 days with poly(I:C) and grew them in the normoxic condition for 6 additional hours before harvesting. We found that indeed the activation of phospho-STAT1 in response to the poly(I:C) stimulus is dampened in cells cultured in hypoxia (Figure S5B). We then evaluated whether HIF activity is needed and used CRISPR-Cas9 to delete ARNT, the HIF1α and HIF2α heterodimerization partner that is essential for the transcriptional activity of HIFs(Semenza, 2012b) (Figure 6A). ARNT knockout (KO) in MCF7 cells led to the inability of hypoxia to induce the expression of NDRG1, a target of both HIF1 and HIF2(Wang et al., 2013) (Figure 6B). However, IFN target gene expression was reduced in response to hypoxia both in

control and ARNT-KO cells (Figures 6B and S5C), suggesting that the effect of hypoxia on IFN signaling is independent of HIF.

Recent reports have shown that, similar to the prolyl hydroxylase domain proteins (PHDs) that hydroxylate HIF in well oxygenated environments, other proteins of the 2-oxoglutarate-dependent dioxygenase family, including some histone demethylases, show low oxygen affinity (high K_M), enabling them to sense physiological changes in oxygen(Batie et al., 2019b; Chakraborty et al., 2019). As a result, hypoxic culture decreases the activity of such histone demethylases, leading to increased levels of methylation in several H3 residues (Figure S5D). KDM6A, KDM5A and KDM4B are 3 of the histone demethylases with the highest K_M for oxygen(Chakraborty et al., 2019). To determine if inhibition of these histone demethylases can mimic the effect of hypoxia on interferon target genes, we treated MCF7 cells with small molecule inhibitors that specifically target these enzymes. Treatment with the KDM6 inhibitor GSK-J4(Heinemann et al., 2014) increased H3K27 trimethylation, but actually enhanced IFN target gene expression (Figures S5E-F). Similarly, MCF7 cells treated with the KDM5 inhibitor KDM5-C70(Tumber et al., 2017) that increases H3K4me3 showed small but significant increases in IFN target gene expression (Figure S5G-H). The KDM4 inhibitor NSC636819(Chu et al., 2014) promoted a modest increase in H3K9me3 levels (Figure S5i). NSC636819 treatment failed to mimic the effect of hypoxia on IFN target genes (Figure S5J), although it did downregulate ESR1 and its target gene PS2 (Figure S5K), as reported elsewhere(Gaughan et al., 2013; Shi et al., 2011). These data suggest that the reduced activities of KDMs are not directly responsible for suppressing the IFN/AP signal.

We then explored the possibility of hypoxia influencing IFN signaling through a PHD dependent but HIF-independent mechanism(Strowitzki et al., 2019). Treatment with the PHD inhibitor FG4592(Provenzano et al., 2016) led to HIF1α stabilization and induction of HIF target genes in MCF7 (Figure S6A-B) and T47D cells (Figure S6C-E), showing that the drug is efficient in inhibiting PHD activity. Cells treated with this small molecule also exhibited lower expression of IFN target genes (Figures 6C and S6D). Because a PHD inhibitor reduced expression of IFN target genes and the absence of ARNT did not impact the hypoxic downregulation of those genes (Figures 6B and S5C), we infer that PHDs control IFN signaling in a HIF-independent manner.

To explore other potential transcription factors that can mediate hypoxia-induced IFN/AP suppression, we performed ATAC-seq analysis of BRx68 cells cultured in hypoxia and normoxia for 8 weeks. In hypoxia, differentially opened regions showed enrichment of many transcription factor motifs for various forkhead box (FOX) proteins (Table S8). Based on a previous report establishing FOXO3 as a confirmed hydroxylation target of PHD1 and FOXO1 a likely one(Zheng et al., 2014), we therefore analyzed a few FOX proteins for their levels in normoxia and hypoxia in MCF7 cells. Although FOXA1 and FOXO3 both showed increased levels in hypoxia, their upregulations are HIF-dependent, as ARNT-KO cells eliminated the effect (Figure S6F). In contrast, the upregulation of FOXO1 protein levels in hypoxia is HIF-independent (Figure 6D) and doesn't involve significant changes in mRNA level (Figure S6G). A similar increase was also seen in other breast cancer cell lines (Figure S6H). In addition, the increase of FOXO1 in hypoxia can be maintained after 3 days of reoxygenation following 14 days of hypoxia, particularly at 4% oxygen (Figure 6E). We then designed several sgRNAs against the promoter of FOXO1 gene and used CRISPR-mediated silencing (CRISPRi) to suppress the level

of FOXO1 (Figures S6I and 6F). FOXO1 suppression led to increased levels of the IFN upstream transcription factor, interferon regulatory factor 3 (IRF3) (Figures S6I and 6F), consistent with a previous report(Lei et al., 2013). Importantly, FOXO1 suppression led to significant upregulation of IFN target IFIT1 expression in both normoxia and hypoxia (Figure 6G). Furthermore, the PHD inhibitor FG4592 upregulated FOXO1 protein level in MCF7 cells (Figure 6H), and knocking down FOXO1 rescued FG4592-induced suppression of IFN target (Figure 6I), in a pattern similar to that in hypoxia (Figure 6G). These results showed that PHD-dependent regulation of FOXO1 may at least partially explain the HIF-independent effect of the hypoxic downregulation of IFN/AP.

Erasing hypoxic memory enhances immune clearance when combined with immune checkpoint inhibitors.

To investigate the potential involvement of epigenetic regulation in the hypoxic memory of IFN/AP suppression, we evaluated the ability of several epigenetic inhibitors to rescue IFN/AP suppression after reoxygenation. An HDACi, MS275 (Entinostat)(Saito et al., 1999), and a low concentration of a G9a/GLP inhibitor, UNC0638(Vedadi et al., 2011), reversed the hypoxic memory of IFN target IFIT1 (Figures 7A-B and S7A). In contrast, MS275 did not show a clear rescue of the immediate hypoxic suppression of the IFIT1 level in the 3-day hypoxic culture (Figure S7B). To evaluate the effect *in vivo*, we performed scRNAseq analysis of the NT2.5 cells in syngeneic tumors treated with vehicle, Entinostat alone, or in combination with anti-CTLA4, anti-PD1, or both(Christmas et al., 2018). A total of 20 tumors (4 from each group) were processed by 10x Chromium platform after 3 weeks of treatment, but before a significant tumor shrinkage. Decile plots of the tumor cells ranked by IFN/AP score showed a clear inverse

correlation of hypoxia and IFN/AP signatures after Entinostat treatment, and the effect became even more obvious when combined with the immunotherapies (Figure 7C). Compared with vehicle condition, Entinostat treatment shifted these 2 features of the tumor cells. The most obvious change seemed to occur in the population of the vehicle condition with double negative scores for both hypoxia and IFN/AP, which may contain tumor cells that have left the hypoxic region but retain a hypoxic memory of IFN/AP downregulation. It is possible that Entinostat removed the hypoxic memory and upregulated the IFN/AP signals for tumor cells in the normoxic region (negative for hypoxia). This corroborates the above *in vitro* finding of Entinostat erasing the hypoxic memory of IFN target suppression, but not so significantly in hypoxic conditions. The combination of Entinostat with checkpoint blockades led to an overall increased hypoxia score in the tumors (Figure S7C), suggesting more effective elimination of cells in normoxia. Indeed, NT2.5 cells showed hypoxic memory of IFN target suppression after reoxygenation (Figure 7D). When NT2.5 cells grown in normoxia or hypoxia (4% or 1% O_2) for 14 days were injected in immunocompetent FVB mice, cells pre-cultured in 1% hypoxia generated significantly bigger tumors, compared to those pre-cultured in normoxia (Figure 7E), accompanied with more immunosuppressive Arginase (Arg)+ granulocytic myeloid derived suppressor cells (gMDSCs) and macrophages (Figures 7F-G and S7D-G). These data suggest that besides the intrinsic effect on the tumor cells, this hypoxic memory can modify the recruitment of immune cells to shift the balance towards a more immunosuppressive microenvironment. In addition, Entinostat has the potential to erase hypoxic memory and promote tumor cell clearance, when combined with checkpoint immunotherapies.

Discussion

In this study, we discovered that hypoxia leads to the suppression of type I IFN signaling and downstream AP pathway specifically in the luminal subtype of breast cancer cells. This effect is mediated via HIF-independent but PHD-dependent mechanisms, including the FOXO1 mediated suppression of IRF3. Intriguingly, even after a return to normoxic conditions, from a prolonged exposure to low oxygen levels, hypoxia induced IFN/AP suppression can be maintained as a hypoxic memory, which promotes tumorigenesis and metastasis (Figure 7H). This suggests a novel mechanism for the enhanced metastatic capacity of tumor cells shed from hypoxic regions.

As one of the common tumor microenvironment (TME) features of solid tumors, hypoxia has well-known multifaceted effects that promote tumor progression(Rankin et al., 2016). Our finding on its effect in suppressing tumor cell intrinsic type I IFN and AP signals provides an additional novel mechanism. Type I IFN signaling has intrinsic tumor suppressive effect, by inhibiting proliferation and promoting apoptosis, and it also plays a key role in immune surveillances against tumors(Snell et al., 2017). Therefore, by downregulating intrinsic type I IFN as well as downstream AP machinery, hypoxia provides tumor cell intrinsic and extrinsic benefits during tumor progression. Of note, a study with similar topic has recently been reported(Miar et al., 2020), however with different results. Whereas this report showed similar effects in all subtypes(Miar et al., 2020), we found that this hypoxia mediated suppression of IFN/AP to be specific in luminal subtypes of breast cancer cells with no obvious difference in basal subtype cell lines. The differences may be due to the level of hypoxia used in the experiments. We mainly focused on relatively mild hypoxia condition (4%-1% O_2) since this is likely to be more common across tumor types(Muz et al., 2015), while a much lower oxygen levels (1%-0.1%) have been used in the other report(Miar et al., 2020). Intriguingly, we did

observe differences in the long term effect by different hypoxia priming, highlighting the importance in considering the specific niche effects. Moreover, our scRNAseq analysis of the MMTV-PyMT tumor model further supports such effect being more prominent in luminal characteristic tumor cells based on the report that MMTV-PyMT model progresses with a loss of luminal features over time(Lin et al., 2003). scRNAseq analysis of other syngeneic breast cancer models also showed a clear inverse correlation of hypoxia and IFN/AP scores in tumor cells sorted based on Cd24 surface marker likely enriching luminal type of tumor cells(Yeo et al., 2020). However, the exact mechanisms underlying the luminal versus basal subtypes in terms of their hypoxic responses are not yet clear and warrants further investigation, which may contribute to a better understanding of why luminal tumors are immune "colder" tumors than the basal subtypes.

We also found that hypoxia downregulates IFN/AP signal in a HIF-independent manner. Epigenetic factors may play an indirect role since we observed changes in global histone methylations in hypoxia. Epigenetic mechanisms indeed contribute to hypoxic memory maintenances. Different from previously mentioned mechanism in which mitochondrial dsRNA quantity is reduced in hypoxia compared to normoxia(Arnaiz et al., 2020), we did not detect significant differences in the mitochondrial dsRNA levels. Instead, we found that upregulated level of FOXO1 protein in hypoxia likely promotes degradation of IRF3 thereby reducing levels of downstream IFN targets. A previous report has identified that FOXO1 is a potential hydroxylated target of PHD1(Zheng et al., 2014), which could explain the PHD-dependent but HIF-independent effect that we have seen. FOXO transcription factors are mostly viewed as tumor suppressors based on their well-known transcriptional role in regulating cell cycle,

apoptosis, metabolism, and scavenging reactive oxygen species for maintaining cellular homeostasis(Jiramongkol and Lam, 2020). However, recent studies have proposed controversial results suggesting their tumor promoting roles(Hornsveld et al., 2018b, 2018a). In addition, the potential role of FOXO in the cytoplasm is not well understood. In lights of a previous reported cytoplasm role of FOXO1 in degrading IRF3 in anti-viral context(Lei et al., 2013), and our data supporting a similar inverse correlation of FOXO1 and IRF3 protein levels, it will be worth further investigating the exact localization and mechanism of FOXO1 in hypoxic conditions. Moreover, tumor cells go through distinct signaling and physical challenges during the metastatic cascade and FOXO proteins are known to be regulated mostly at posttranslational level by many signals, deciphering the role of FOXOs in different contexts will shed light into their role during different steps of metastasis. In a different line of investigation supporting this notion, some of the similar processes that play tumor suppressing role for primary tumorigenesis are now being proposed as having promoting role for metastasis, such as antioxidants in promoting CTC survival and metastatic colonization(Gal et al., 2015; Piskounova et al., 2015; Teng et al., 2020).

Our intriguing finding of hypoxic memory of IFN/AP suppression is, to the best of our knowledge, the first reported long term suppression of such signal. During our manuscript preparation, a study has utilized a similar 2-plasmid Cre-loxP mediated hypoxia tracing system to evaluate the long-term effect of hypoxia *in vivo*(Godet et al., 2019). The study noted a long-term effect of hypoxia that promotes metastasis, but only utilized the basal subtype of breast cancer cells. In that context, the hypoxic memory mainly persists via upregulated genes that promote cell survival in the presence of high levels of ROS. As we have shown that hypoxia-

mediated IFN/AP suppression is prominent in luminal subtype, it is likely that the signals lasting longer as hypoxic memory is subtype dependent and mechanisms could be heterogeneous. A surprising finding is that mild (4% O_2) and long term (14 days) of hypoxia exposure, but not severe (1% O_2), nor a short exposure (3 days), lead to the prolonged memory of IFN/AP suppression in MCF7 cells. While in NT2.5 cells, hypoxic memory can be established by both mild and severe hypoxia conditions. The unique hypoxia priming condition suggests specific molecular mechanisms are involved in establishing and/or maintaining such cellular memory in a cell type dependent manner, which warrants further analysis.

Within solid tumors, hypoxic features constantly change due to tumor growth and cellular movement. Hypoxic memory of IFN/AP suppression could contribute to immune evasion and reduce efficacy of checkpoint immunotherapies. As shown in our *in vitro* MCF7 data and *in vivo* data of NT2.5 syngeneic tumors, Entinostat upregulates IFN/AP signals of cells in normoxic regions, resulting in increased hypoxia scores when combined with immunocheckpoint treatment. Despite the limitation of one static time point and the correlative nature, the data suggests the possibility that for NT2.5 cells with hypoxic memory (ie. low IFN/AP score in the normoxia region) in vehicle condition, such memory can be "erased" by Entinostat treatment thereby leading to improved immune clearance of cells in normoxic area by the immune checkpoint therapies. A more direct link with multiple time points will be worth evaluating in future studies. Moreover, our data of the syngeneic model showed that NT2.5 cells pre-conditioned in hypoxia lead to bigger tumor formation, with recruitment of more immunosuppressive cell types in the TME. Furthermore, the prolonged suppression of IFN/AP would likely also contribute to the immune evasive feature commonly seen in CTCs. Indeed,

after exposure to hypoxia, only those CTCs with the capacity for a hypoxic memory of IFN/AP suppression showed enhanced tumorigenesis and metastasis. Our study suggests a novel concept of hypoxia induced long term cellular memory as a potential mechanism for promoting the metastatic capacity of CTCs.

References

Aguilera, T.A., Rafat, M., Castellini, L., Shehade, H., Kariolis, M.S., Hui, A.B.-Y., Stehr, H., Eyben, R. von, Jiang, D., Ellies, L.G., et al. (2016). Reprogramming the immunological microenvironment through radiation and targeting Axl. Nat. Commun. *7*, 13898.

Aguilera, T.A., Elghonaimy, E.A., Shehade, H., Rafat, M., Castellini, L., Jiang, D., Kariolis, M., Koong, A.C., Le, Q.-T., Ellies, L.G., et al. (2020). Induced Tumor Heterogeneity Reveals Factors Informing Radiation and Immunotherapy Combinations. Clin. Cancer Res. *26*, 2972–2985.

Anders, S., Pyl, P.T., and Huber, W. (2015). HTSeq--a Python framework to work with high-throughput sequencing data. Bioinforma. Oxf. Engl. *31*, 166–169.

Arnaiz, E., Miar, A., Dias, A.G., Prasad, N., Schulze, U., Waithe, D., Rehwinkel, J., and Harris, A.L. (2020). Hypoxia regulates endogenous double-stranded RNA production via reduced mitochondrial DNA transcription. BioRxiv 2020.07.31.230300.

Batie, M., Frost, J., Frost, M., Wilson, J.W., Schofield, P., and Rocha, S. (2019a). Hypoxia induces rapid changes to histone methylation and reprograms chromatin. Science *363*, 1222–1226.

Batie, M., Frost, J., Frost, M., Wilson, J.W., Schofield, P., and Rocha, S. (2019b). Hypoxia induces rapid changes to histone methylation and reprograms chromatin. Science *363*, 1222–1226.

Bertout, J.A., Patel, S.A., and Simon, M.C. (2008). The impact of O 2 availability on human cancer. Nat. Rev. Cancer *8*, 967–975.

Boukhaled, G.M., Harding, S., and Brooks, D.G. (2021). Opposing Roles of Type I Interferons in Cancer Immunity. Annu. Rev. Pathol. Mech. Dis. *16*, 167–198.

Bruick, R.K., and McKnight, S.L. (2001). A Conserved Family of Prolyl-4-Hydroxylases That Modify HIF. Science *294*, 1337–1340.

Buenrostro, J.D., Wu, B., Chang, H.Y., and Greenleaf, W.J. (2015). ATAC-seq: A Method for Assaying Chromatin Accessibility Genome-Wide. Curr. Protoc. Mol. Biol. *109*, 21.29.1-21.29.9.

Buffa, F.M., Harris, A.L., West, C.M., and Miller, C.J. (2010). Large meta-analysis of multiple cancers reveals a common, compact and highly prognostic hypoxia metagene. Br. J. Cancer *102*, 428–435.

Chakraborty, A.A., Laukka, T., Myllykoski, M., Ringel, A.E., Booker, M.A., Tolstorukov, M.Y., Meng, Y.J., Meier, S.R., Jennings, R.B., Creech, A.L., et al. (2019). Histone demethylase KDM6A directly senses oxygen to control chromatin and cell fate. Science *363*, 1217–1222.

Chiu, D.K.-C., Tse, A.P.-W., Xu, I.M.-J., Di Cui, J., Lai, R.K.-H., Li, L.L., Koh, H.-Y., Tsang, F.H.-C., Wei, L.L., Wong, C.-M., et al. (2017). Hypoxia inducible factor HIF-1 promotes myeloid-derived suppressor cells accumulation through ENTPD2/CD39L1 in hepatocellular carcinoma. Nat. Commun. *8*, 517.

Chouaib, S., Noman, M.Z., Kosmatopoulos, K., and Curran, M.A. (2017). Hypoxic stress: obstacles and opportunities for innovative immunotherapy of cancer. Oncogene *36*, 439–445.

Choudhry, H., and Harris, A.L. (2017). Advances in Hypoxia-Inducible Factor Biology. Cell Metab.

Christmas, B.J., Rafie, C.I., Hopkins, A.C., Scott, B.A., Ma, H.S., Cruz, K.A., Woolman, S., Armstrong, T.D., Connolly, R.M., Azad, N.A., et al. (2018). Entinostat Converts Immune-Resistant Breast and Pancreatic Cancers into Checkpoint-Responsive Tumors by Reprogramming Tumor-Infiltrating MDSCs. Cancer Immunol. Res. *6*, 1561–1577.

Chu, C.-H., Wang, L.-Y., Hsu, K.-C., Chen, C.-C., Cheng, H.-H., Wang, S.-M., Wu, C.-M., Chen, T.-J., Li, L.-T., Liu, R., et al. (2014). KDM4B as a Target for Prostate Cancer: Structural Analysis and Selective Inhibition by a Novel Inhibitor. J. Med. Chem. *57*, 5975–5985.

Dobin, A., Davis, C.A., Schlesinger, F., Drenkow, J., Zaleski, C., Jha, S., Batut, P., Chaisson, M., and Gingeras, T.R. (2013). STAR: ultrafast universal RNA-seq aligner. Bioinforma. Oxf. Engl. *29*, 15–21.

Donato, C., Kunz, L., Castro-Giner, F., Paasinen-Sohns, A., Strittmatter, K., Szczerba, B.M., Scherrer, R., Maggio, N.D., Heusermann, W., Biehlmaier, O., et al. (2020). Hypoxia Triggers the Intravasation of Clustered Circulating Tumor Cells. Cell Rep. *32*.

Eisinger-Mathason, T.S.K., Zhang, M., Qiu, Q., Skuli, N., Nakazawa, M.S., Karakasheva, T., Mucaj, V., Shay, J.E.S., Stangenberg, L., Sadri, N., et al. (2013). Hypoxia-Dependent Modification of Collagen Networks Promotes Sarcoma Metastasis. Cancer Discov. *3*, 1190–1205.

Erler, J.T., Bennewith, K.L., Cox, T.R., Lang, G., Bird, D., Koong, A., Le, Q.-T., and Giaccia, A.J. (2009). Hypoxia-Induced Lysyl Oxidase Is a Critical Mediator of Bone Marrow Cell Recruitment to Form the Premetastatic Niche. Cancer Cell *15*, 35–44.

Fischer, K., Hoffmann, P., Voelkl, S., Meidenbauer, N., Ammer, J., Edinger, M., Gottfried, E., Schwarz, S., Rothe, G., Hoves, S., et al. (2007). Inhibitory effect of tumor cell–derived lactic acid on human T cells. Blood *109*, 3812–3819.

Gal, K.L., Ibrahim, M.X., Wiel, C., Sayin, V.I., Akula, M.K., Karlsson, C., Dalin, M.G., Akyürek, L.M., Lindahl, P., Nilsson, J., et al. (2015). Antioxidants can increase melanoma metastasis in mice. Sci. Transl. Med. *7*, 308re8-308re8.

Gaughan, L., Stockley, J., Coffey, K., O'Neill, D., Jones, D.L., Wade, M., Wright, J., Moore, M., Tse, S., Rogerson, L., et al. (2013). KDM4B is a Master Regulator of the Estrogen Receptor Signalling Cascade. Nucleic Acids Res. *41*, 6892–6904.

Godet, I., Shin, Y.J., Ju, J.A., Ye, I.C., Wang, G., and Gilkes, D.M. (2019). Fate-mapping post-hypoxic tumor cells reveals a ROS-resistant phenotype that promotes metastasis. Nat. Commun. *10*, 4862.

Harada, H., Inoue, M., Itasaka, S., Hirota, K., Morinibu, A., Shinomiya, K., Zeng, L., Ou, G., Zhu, Y., Yoshimura, M., et al. (2012). Cancer cells that survive radiation therapy acquire HIF-1 activity and translocate towards tumour blood vessels. Nat. Commun. *3*, 783.

Hatfield, S.M., Kjaergaard, J., Lukashev, D., Schreiber, T.H., Belikoff, B., Abbott, R., Sethumadhavan, S., Philbrook, P., Ko, K., Cannici, R., et al. (2015). Immunological mechanisms of the antitumor effects of supplemental oxygenation. Sci. Transl. Med. *7*, 277ra30-277ra30.

Heinemann, B., Nielsen, J.M., Hudlebusch, H.R., Lees, M.J., Larsen, D.V., Boesen, T., Labelle, M., Gerlach, L.-O., Birk, P., and Helin, K. (2014). Inhibition of demethylases by GSK-J1/J4. Nature *514*, E1–E2.

Hornsveld, M., Dansen, T.B., Derksen, P.W., and Burgering, B.M.T. (2018a). Re-evaluating the role of FOXOs in cancer. Semin. Cancer Biol. *50*, 90–100.

Hornsveld, M., Smits, L.M.M., Meerlo, M., Amersfoort, M. van, Koerkamp, M.J.A.G., Leenen, D. van, Kloet, D.E.A., Holstege, F.C.P., Derksen, P.W.B., Burgering, B.M.T., et al. (2018b). FOXO Transcription Factors Both Suppress and Support Breast Cancer Progression. Cancer Res. *78*, 2356–2369.

Huang, L.E., Gu, J., Schau, M., and Bunn, H.F. (1998). Regulation of hypoxia-inducible factor 1α is mediated by an O2-dependent degradation domain via the ubiquitin-proteasome pathway. Proc. Natl. Acad. Sci. *95*, 7987–7992.

Iriondo, O., Rábano, M., Domenici, G., Carlevaris, O., López-Ruiz, J.A., Zabalza, I., Berra, E., Vivanco, M. dM, Iriondo, O., Rábano, M., et al. (2015). Distinct breast cancer stem/progenitor cell populations require either HIF1α or loss of PHD3 to expand under hypoxic conditions. Oncotarget *6*, 31721–31739.

Ivan, M., and Kaelin, W.G. (2017). The EGLN-HIF O 2 -Sensing System: Multiple Inputs and Feedbacks. Mol. Cell *66*, 772–779.

Ivan, M., Kondo, K., Yang, H., Kim, W., Valiando, J., Ohh, M., Salic, A., Asara, J.M., Lane, W.S., and Jr, W.G.K. (2001). HIFα Targeted for VHL-Mediated Destruction by Proline Hydroxylation: Implications for O2 Sensing. Science *292*, 464–468.

Jiramongkol, Y., and Lam, E.W.-F. (2020). FOXO transcription factor family in cancer and metastasis. Cancer Metastasis Rev. *39*, 681–709.

Jolma, A., Yan, J., Whitington, T., Toivonen, J., Nitta, K.R., Rastas, P., Morgunova, E., Enge, M., Taipale, M., Wei, G., et al. (2013). DNA-binding specificities of human transcription factors. Cell *152*, 327–339.

Kaelin, W.G., and Ratcliffe, P.J. (2008). Oxygen Sensing by Metazoans: The Central Role of the HIF Hydroxylase Pathway. Mol. Cell *30*, 393–402.

Klotz, R., Thomas, A., Teng, T., Han, S.M., Iriondo, O., Li, L., Restrepo-Vassalli, S., Wang, A., Izadian, N., MacKay, M., et al. (2020). Circulating Tumor Cells Exhibit Metastatic Tropism and Reveal Brain Metastasis Drivers. Cancer Discov. *10*, 86–103.

Kuchnio, A., Moens, S., Bruning, U., Kuchnio, K., Cruys, B., Thienpont, B., Broux, M., Ungureanu, A.A., Leite de Oliveira, R., Bruyère, F., et al. (2015). The Cancer Cell Oxygen Sensor PHD2 Promotes Metastasis via Activation of Cancer-Associated Fibroblasts. Cell Rep. *12*, 992–1005.

Langmead, B., and Salzberg, S.L. (2012). Fast gapped-read alignment with Bowtie 2. Nat. Methods *9*, 357–359.

Lei, C.-Q., Zhang, Y., Xia, T., Jiang, L.-Q., Zhong, B., and Shu, H.-B. (2013). FoxO1 Negatively Regulates Cellular Antiviral Response by Promoting Degradation of IRF3*,. J. Biol. Chem. *288*, 12596–12604.

Li, Z., Bao, S., Wu, Q., Wang, H., Eyler, C., Sathornsumetee, S., Shi, Q., Cao, Y., Lathia, J., McLendon, R.E., et al. (2009). Hypoxia-Inducible Factors Regulate Tumorigenic Capacity of Glioma Stem Cells. Cancer Cell *15*, 501–513.

Liao, Y., Smyth, G.K., and Shi, W. (2014). featureCounts: an efficient general purpose program for assigning sequence reads to genomic features. Bioinformatics *30*, 923–930.

Lin, E.Y., Jones, J.G., Li, P., Zhu, L., Whitney, K.D., Muller, W.J., and Pollard, J.W. (2003). Progression to Malignancy in the Polyoma Middle T Oncoprotein Mouse Breast Cancer Model Provides a Reliable Model for Human Diseases. Am. J. Pathol. *163*, 2113–2126.

Love, M.I., Huber, W., and Anders, S. (2014). Moderated estimation of fold change and dispersion for RNA-seq data with DESeq2. Genome Biol. *15*, 550.

Miar, A., Arnaiz, E., Bridges, E., Beedie, S., Cribbs, A.P., Downes, D.J., Beagrie, R.A., Rehwinkel, J., and Harris, A.L. (2020). Hypoxia Induces Transcriptional and Translational Downregulation of the Type I IFN Pathway in Multiple Cancer Cell Types. Cancer Res. *80*, 5245–5256.

Mootha, V.K., Lindgren, C.M., Eriksson, K.-F., Subramanian, A., Sihag, S., Lehar, J., Puigserver, P., Carlsson, E., Ridderstråle, M., Laurila, E., et al. (2003). PGC-1alpha-responsive genes involved in oxidative phosphorylation are coordinately downregulated in human diabetes. Nat. Genet. *34*, 267–273.

Movahedi, K., Laoui, D., Gysemans, C., Baeten, M., Stangé, G., Bossche, J.V. den, Mack, M., Pipeleers, D., Veld, P.I., Baetselier, P.D., et al. (2010). Different Tumor Microenvironments

Contain Functionally Distinct Subsets of Macrophages Derived from Ly6C(high) Monocytes. Cancer Res. *70*, 5728–5739.

Muz, B., de la Puente, P., Azab, F., and Azab, A.K. (2015). The role of hypoxia in cancer progression, angiogenesis, metastasis, and resistance to therapy. Hypoxia *3*, 83–92.

Parker, B.S., Rautela, J., and Hertzog, P.J. (2016). Antitumour actions of interferons: implications for cancer therapy. Nat. Rev. Cancer *16*, 131–144.

Piskounova, E., Agathocleous, M., Murphy, M.M., Hu, Z., Huddlestun, S.E., Zhao, Z., Leitch, A.M., Johnson, T.M., DeBerardinis, R.J., and Morrison, S.J. (2015). Oxidative stress inhibits distant metastasis by human melanoma cells. Nature *527*, 186–191.

Provenzano, R., Besarab, A., Sun, C.H., Diamond, S.A., Durham, J.H., Cangiano, J.L., Aiello, J.R., Novak, J.E., Lee, T., Leong, R., et al. (2016). Oral Hypoxia–Inducible Factor Prolyl Hydroxylase Inhibitor Roxadustat (FG-4592) for the Treatment of Anemia in Patients with CKD. Clin. J. Am. Soc. Nephrol. CJASN *11*, 982–991.

Pugh, C.W., and Ratcliffe, P.J. (2003). Regulation of angiogenesis by hypoxia: role of the HIF system. Nat. Med. *9*, 677–684.

Quinlan, A.R., and Hall, I.M. (2010). BEDTools: a flexible suite of utilities for comparing genomic features. Bioinformatics *26*, 841–842.

Rankin, E.B., Nam, J.-M., and Giaccia, A.J. (2016). Hypoxia: Signaling the Metastatic Cascade. Trends Cancer *2*, 295–304.

Ritchie, M.E., Phipson, B., Wu, D., Hu, Y., Law, C.W., Shi, W., and Smyth, G.K. (2015). limma powers differential expression analyses for RNA-sequencing and microarray studies. Nucleic Acids Res. *43*, e47.

Saito, A., Yamashita, T., Mariko, Y., Nosaka, Y., Tsuchiya, K., Ando, T., Suzuki, T., Tsuruo, T., and Nakanishi, O. (1999). A synthetic inhibitor of histone deacetylase, MS-27-275, with marked in vivo antitumor activity against human tumors. Proc. Natl. Acad. Sci. *96*, 4592–4597.

Sandelin, A., Alkema, W., Engström, P., Wasserman, W.W., and Lenhard, B. (2004). JASPAR: an open-access database for eukaryotic transcription factor binding profiles. Nucleic Acids Res. *32*, D91–D94.

Satija, R., Farrell, J.A., Gennert, D., Schier, A.F., and Regev, A. (2015). Spatial reconstruction of single-cell gene expression data. Nat. Biotechnol. *33*, 495–502.

Semenza, G.L. (2012a). Hypoxia-Inducible Factors in Physiology and Medicine. Cell *148*, 399–408.

Semenza, G.L. (2012b). Hypoxia-Inducible Factors in Physiology and Medicine. Cell *148*, 399–408.

Shi, L., Sun, L., Li, Q., Liang, J., Yu, W., Yi, X., Yang, X., Li, Y., Han, X., Zhang, Y., et al. (2011). Histone demethylase JMJD2B coordinates H3K4/H3K9 methylation and promotes hormonally responsive breast carcinogenesis. Proc. Natl. Acad. Sci. *108*, 7541–7546.

Smith, A.D., Sumazin, P., Xuan, Z., and Zhang, M.Q. (2006). DNA motifs in human and mouse proximal promoters predict tissue-specific expression. Proc. Natl. Acad. Sci. U. S. A. *103*, 6275–6280.

Snell, L.M., McGaha, T.L., and Brooks, D.G. (2017). Type I Interferon in Chronic Virus Infection and Cancer. Trends Immunol. *38*, 542–557.

Song, H., Shahverdi, K., Huso, D.L., Wang, Y., Fox, J.J., Hobbs, R.F., Gimi, B., Gabrielson, K.L., Pomper, M.G., Tsui, B.M., et al. (2008). An Immunotolerant HER-2/neu Transgenic Mouse Model of Metastatic Breast Cancer. Clin. Cancer Res. *14*, 6116–6124.

Strowitzki, M.J., Cummins, E.P., and Taylor, C.T. (2019). Protein Hydroxylation by Hypoxia-Inducible Factor (HIF) Hydroxylases: Unique or Ubiquitous? Cells *8*, 384.

Subramanian, A., Tamayo, P., Mootha, V.K., Mukherjee, S., Ebert, B.L., Gillette, M.A., Paulovich, A., Pomeroy, S.L., Golub, T.R., Lander, E.S., et al. (2005). Gene set enrichment analysis: a knowledge-based approach for interpreting genome-wide expression profiles. Proc. Natl. Acad. Sci. U. S. A. *102*, 15545–15550.

Teng, T., Kamal, M., Iriondo, O., Amzaleg, Y., Luo, C., Thomas, A., Lee, G., Hsu, C.-J., Nguyen, J.D., Kang, I., et al. (2020). N-Acetyl-L-cysteine Promotes Ex Vivo Growth and Expansion of Single Circulating Tumor Cells by Mitigating Cellular Stress Responses. Mol. Cancer Res.

Thienpont, B., Steinbacher, J., Zhao, H., D'Anna, F., Kuchnio, A., Ploumakis, A., Ghesquière, B., Dyck, L.V., Boeckx, B., Schoonjans, L., et al. (2016). Tumour hypoxia causes DNA hypermethylation by reducing TET activity. Nature *537*, 63.

Tumber, A., Nuzzi, A., Hookway, E.S., Hatch, S.B., Velupillai, S., Johansson, C., Kawamura, A., Savitsky, P., Yapp, C., Szykowska, A., et al. (2017). Potent and Selective KDM5 Inhibitor Stops Cellular Demethylation of H3K4me3 at Transcription Start Sites and Proliferation of MM1S Myeloma Cells. Cell Chem. Biol. *24*, 371–380.

Van Overmeire, E., Laoui, D., Keirsse, J., Van Ginderachter, J.A., and Sarukhan, A. (2014). Mechanisms Driving Macrophage Diversity and Specialization in Distinct Tumor Microenvironments and Parallelisms with Other Tissues. Front. Immunol. *5*.

Varia, M.A., Calkins-Adams, D.P., Rinker, L.H., Kennedy, A.S., Novotny, D.B., Fowler, W.C., and Raleigh, J.A. (1998). Pimonidazole: A Novel Hypoxia Marker for Complementary Study of Tumor Hypoxia and Cell Proliferation in Cervical Carcinoma. Gynecol. Oncol. *71*, 270–277.

Vedadi, M., Barsyte-Lovejoy, D., Liu, F., Rival-Gervier, S., Allali-Hassani, A., Labrie, V., Wigle, T.J., DiMaggio, P.A., Wasney, G.A., Siarheyeva, A., et al. (2011). A chemical probe selectively inhibits G9a and GLP methyltransferase activity in cells. Nat. Chem. Biol. *7*, 566–574.

Vito, A., El-Sayes, N., and Mossman, K. (2020). Hypoxia-Driven Immune Escape in the Tumor Microenvironment. Cells *9*, 992.

Wang, Q., Li, L.-H., Gao, G.-D., Wang, G., Qu, L., Li, J.-G., and Wang, C.-M. (2013). HIF-1α up-regulates NDRG1 expression through binding to NDRG1 promoter, leading to proliferation of lung cancer A549 cells. Mol. Biol. Rep. *40*, 3723–3729.

Wong, C.C.-L., Gilkes, D.M., Zhang, H., Chen, J., Wei, H., Chaturvedi, P., Fraley, S.I., Wong, C.-M., Khoo, U.-S., Ng, I.O.-L., et al. (2011). Hypoxia-inducible factor 1 is a master regulator of breast cancer metastatic niche formation. Proc. Natl. Acad. Sci. *108*, 16369–16374.

Yang, M.-H., Wu, M.-Z., Chiou, S.-H., Chen, P.-M., Chang, S.-Y., Liu, C.-J., Teng, S.-C., and Wu, K.-J. (2008). Direct regulation of TWIST by HIF-1α promotes metastasis. Nat. Cell Biol. *10*, 295–305.

Yeo, S.K., Zhu, X., Okamoto, T., Hao, M., Wang, C., Lu, P., Lu, L.J., and Guan, J.-L. (2020). Single-cell RNA-sequencing reveals distinct patterns of cell state heterogeneity in mouse models of breast cancer. ELife *9*, e58810.

Yu, M., Bardia, A., Wittner, B.S., Stott, S.L., Smas, M.E., Ting, D.T., Isakoff, S.J., Ciciliano, J.C., Wells, M.N., Shah, A.M., et al. (2013). Circulating breast tumor cells exhibit dynamic changes in epithelial and mesenchymal composition. Science *339*, 580–584.

Yu, M., Bardia, A., Aceto, N., Bersani, F., Madden, M.W., Donaldson, M.C., Desai, R., Zhu, H., Comaills, V., Zheng, Z., et al. (2014). Ex vivo culture of circulating breast tumor cells for individualized testing of drug susceptibility. Science *345*, 216–220.

Zhang, Y., Liu, T., Meyer, C.A., Eeckhoute, J., Johnson, D.S., Bernstein, B.E., Nusbaum, C., Myers, R.M., Brown, M., Li, W., et al. (2008). Model-based Analysis of ChIP-Seq (MACS). Genome Biol. *9*, 1–9.

Zheng, X., Zhai, B., Koivunen, P., Shin, S.J., Lu, G., Liu, J., Geisen, C., Chakraborty, A.A., Moslehi, J.J., Smalley, D.M., et al. (2014). Prolyl hydroxylation by EglN2 destabilizes FOXO3a by blocking its interaction with the USP9x deubiquitinase. Genes Dev. *28*, 1429–1444.

Babraham Bioinformatics - Trim Galore!

Acknowledgements. We thank the USC Flow Cytometry Facility and USC Molecular Genomics Core for their technical support; D. Ruble and members of CHLA Molecular Pathology Genomics Core for technical assistance; Drs. J. Lang and T. Aguilera for providing cell lines; Drs. Q. Zhang and H. Harada for providing reagents; C. Lytal for editing the manuscript. This research was supported by the following: The National Institutes of Health (NIH) grant DP2 CA206653 (M.Y.), the Stop Cancer Foundation (M.Y.), the PEW Charitable Trusts and the Alexander & Margaret Stewart Trust (M.Y.), the Department of Defense Era of Hope Scholar Award (M.Y.), the Richard Merkin Foundation (M.Y.), the Broad Fellowship (O.I.), and the NIH grant T90DE021982 (trainees D.M. and Y.A.). The project described was supported in part (core facilities) by award number P30CA014089 from the National Cancer Institute.

Author Contributions. O.I. and M.Y. conceived the study. O.I., D.M., Y.L. and M.Y. designed experiments. O.I., D.M., Y.L., A.D., G.L., S.H. and M.Y. performed experiments. O.I., D.M., Y.L., C.R.C., A.T., Y.A., V.O., M.M., A.D., G.L., B.A.B., E.R.T. and M.Y. contributed to analysis and interpretation of data. C.R.C., A.T., Y.A., M.M., A.S. and C.M. conducted computational analyses. E.R.T. provided scRNAseq data of syngeneic tumors. O.I. and M.Y. wrote the manuscript. All authors edited and commented on the manuscript. M.Y. supervised the study.

Methods

Cell culture and reagents

CTC lines derived from patients with luminal breast tumors(Yu et al., 2014) were cultured in ultra-low attachment plates (Corning) with RPMI 1640 supplemented with 20 ng/ml EGF, 20 ng/ml bFGF, 1X B27 and 1X antibiotic/antimycotic. CTCs were maintained in a Nuaire NU-5831 incubator at 4% O_2 and 5% CO_2, and media was changed every 3 or 4 days. For normoxia vs hypoxia experiments, equal number of cells were plated and kept in normoxia or hypoxia (4% O_2) conditions for the indicated duration.

MCF7, MDA-MB-231, HS578T and HEK293T cells were purchased from the American Type Culture Collection and were maintained in DMEM supplemented with 10% FBS. T47D and BT474 cells were provided by Dr. Julie Lang and were cultured in RPMI media with 10% FBS. Py117 and PY8119 cells were provided by Dr. Todd Aguilera and maintained in F12 media containing 5% fetal clone II (Hyclone) and MITO+ (1:1000 dilution, Corning). NT2.5 cells were provided by Dr. Evanthia Roussos Torres and cultured in RPMI media supplemented with 20% FBS, 1.2% Hepes, 1% L-Glutamine, 1% non-essential aminoacids, 1% sodium pyruvate and 0.2% insulin. For normoxia vs hypoxia experiments, cells were moved to hypoxic incubators (Nuaire NU-5831 for 4% O_2, Biospherix ProOx C21 for 1% O_2) 7-8 hours after plating, to ensure that cells had adhered to dish by the time hypoxia treatment started. For the 14-day-long treatments, cells were split every 3 or 4 days and put back in hypoxia once they adhered to the dish. For experiments with small molecule inhibitors, MCF7 or T47D cells were plated, and once cells adhered to the plates, inhibitors were added in fresh media. Inhibitor concentrations and the

duration of the treatments are specified in the figure legends. The inhibitors used in this study were FG-4592 (Selleckchem, S1007), GSK-J4 (Selleckchem, S7070), KDM5-C70 (Xcess Biosciences, M60192-2), NSC636819 (Sigma, 5131996), MS275 (Selleckchem, S1053) and UNC0638 (U4885).

All cultures were routinely (every 1-2 months) tested for mycoplasma contamination using MycoAlert (Lonza). Autosomal STR profiles for cell line authentication were performed by the University of Arizona Genetics Core.

3D culture

MCF7-HypT cells were FACS sorted for $RFP^{+}GFP^{-}$ phenotype. Cells were counted and 20,000 cells were plated in each well of a 24-well ultra-low attachment plate to allow cells to form small aggregates. The following day, Matrigel-collagen mixture was prepared and MCF7-HypT cells were plated into 8-chamber slides (Corning, 354118) following protocol by Nguyen-Ngoc et al (PMID 25245692). Images of spheres were taken the day of plating and every 2-3 days to track the conversion of RFP^{+} cells to GFP^{+} cells over time. Images were taken on a Keyence BZ-9000 fluorescence microscope.

Generation of stable cell lines

PHAGE2-EF1α-LoxP-DsRED-STOP-LoxP-eGFP (Addgene, 62732) and pLKO.1-5xHRE-CRE-ODD plasmids were used for producing MCF7-HypT cells. To generate the pLKO-

5xHRE-CRE-ODD plasmid, pLKO.1-neo (Addgene, 13425) was used as the backbone. The U6 promoter was deleted and replaced with an XbaI site using NEB Q5 site directed mutagenesis kit (NEB Cat# E0554S) with primers forward, 5'-'AAAAATCTAGATGTGGAAAGGACGAAACACC-3'; reverse, 5'-AAAAATCTAGAGAAATAGGCCCTCGGTGAAG-3' according to manufacturer's protocol. The reaction was transformed into chemically competent NEB Stable cells (NEB Cat#C3040H) and the plasmid was verified by restriction enzyme digestion and Sanger sequencing. Subsequent cloning steps were performed to generate pLKO-5xHRE-CRE-ODD by using primers forward, 5'-AAAAAACTAGTGCTAGCGGTAGGCGTGTACGGTGGGAGGTCTATATAAGCAGAGCTC – 3', reverse 5'-AAAAATCTAGAGATCTGACGGTTCACTAAACGAGCTCTGCTTATATAGACC – 3'; forward, 5'- AAAAAGCTAGCTCTAGAACCATGGCCAATTTACTGACCGTACACC-3', reverse, 5'- AAAAAGCTAGCGGCAACTAGAAGGCACAGTCG – 3'; forward, 5'-AAAAAGCTAGCGGTGGAGAGAGAGACAGAGACAG -3', reverse, 5'-AAAAAGCTAGCGGTGGATCCTGCAAAAAGAACAAGTAGC -3', along with the pEF-5xHRE-GFP (Addgene, 46926) and pEF-5xHRE-CRE-ER^{T2}-ODD-myc(Harada et al., 2012) plasmids as templates.

For generating CRISPRi cells, Lenti-dCas9-KRAB-Blast (Addgene, 89567) and pLKO5.sgFOXO1.EFS.tRFP657 plasmids were used. pLKO5.sgFOXO1.EFS.tRFP657 plasmids were produced by cloning guide RNA sequences for the target gene into pLKO5.sgRNA.EFS.tRFP657 (Addgene, 57824). The guide RNA sequences used were the

following: sg101: 5'-CACCGCTGACAGGGCCGCGGACGGA-3', 5'-AAACTCCGTCCGCGGCCCTGTCAGC-3'; sg102: 5'-CACCGGAAGGACGGACGGACGCCG-3', 5'-AAACCGGCGTCCGTCCGTCCTTCC-3' ; sg103: 5'-CACCGCGCAGCGGGCGCGCCGCTG-3', 5'-AAACCAGCGGCGCGCCCGCTGCGC-3'; sg104: 5'-CACCGAACGAAGCCGGTGCGGCGAG-3', 5'-AAACCTCGCCGCACCGGCTTCGTTC-3' ; sg105: 5'-CACCGTCGCGGGGCCATCCACATCG-3', 5'-AAACCGATGTGGATGGCCCCGCGAC-3'; sg106: 5'-CACCGCTGCTGCCTGTTGAATGTGG-3', 5'-AAACCCACATTCAACAGGCAGCAGC-3' .

Lentiviral particles were produced by cotransfecting 293T cells with lentiviral expression vectors in combination with second generation (VSV-G and pCMV-dR.8.91, for pLKO-5xHRE-CRE-ODD, Lenti-dCas9-KRAB-Blast and sgRNA plasmids) or third generation (VSV-G, PMDL and REV, for PHAGE2-EF1α-LoxP-DsRED-STOP-LoxP-eGFP) lentivirus packaging plasmids, using the TransitLT1 transfection reagent (Mirus). Viruses were concentrated with lenti-X concentrator (Clontech). Cell lines to be infected with virus were seeded with 200,000 cells in each well of a 6-well plate. The following day, polybrene (8μg/ml) and concentrated virus were added to each well and incubated overnight. Cells were then selected for infection using puromycin (1 μg/ml), geneticin (0.5 mg/ml) or FACS sorting.

For CRISPR-knockout (KO), guide RNA sequences for ARNT were cloned into pX458 (Addgene, 48138). sgRNA sequences used were based on (chakraborty paper): sgRNA1, 5'-CACCGGGCTATTAAGCGACGGTCA-3', 5'-AAACTGACCGTCGCTTAATAGCCC-3';

sgRNA2, 5'-CACCGAGAAACGGCCATGCGTAAGA-3', 5'-AAACTCTTACGCATGGCCGTTTCTC-3'. Plasmids were transiently transfected into MCF7 cells using Lipofectamine 3000 according to the manufacturer's protocol (ThermoFisher, L3000015). After three days, GFP+ cells were sorted into individual wells for clonal analysis. Alt-R® Genome Editing Detection Kit (IDT Cat#1075932) was used to screen clones for edited genomes within the targeted region and then validated by western blot for gene knockout.

Mouse tumor assays

The animal protocol was approved by the Institutional Animal Care and Use Committee of the University of Southern California. For orthotopic injections, 6 to 8 weeks-old female NSG mice (Jackson Laboratory) were anesthetized with isofluorane and GFP-Luc labelled cells or MCF7-HypT cells resuspended in 1:1 PBS and Matrigel (BD Biosciences) were injected into the fourth mammary fat pad. Tumor growth was evaluated by *in vivo* imaging or by measuring the tumor size with a caliper. Tumor volume was calculated using the formula $V = \pi \times [d^2 \times D] / 6$, were d and D are the minor and major tumor axes respectively. For tail vein injection, 100,000 GFP-Luc expressing cells were injected into the lateral tail vein of 6 to 8 weeks old female NSG mice. Signals from luciferase-tagged cells were monitored biweekly. Mice were imaged using IVIS Lumina II (Perkin Elmer) following intraperitoneal injection of 150 µl of D-Luciferin substrate at 30 mg/ml (Sid Labs). In all cases, mice were supplemented with 0.36 mg 90-day slow release 17β-Estradiol pellets (Innovative Research of America, Cat# NE-121). For tumor formation experiments with NT2.5 cells, 6 to 8 weeks-old female FVB mice (Jackson Laboratory) were used and tumor cells ($1x10^6$) were resuspended in PBS and injected into the fourth mammary fat

pad. For full methods describing derivation of NT2.5 tumors used for scRNAseq please see(Christmas et al., 2018).

Tumor dissociation

Tumors were dissected and collected in cold PBS. A piece of tumor was saved for fixation and immunostaining when needed. Tumors were minced and placed in dissociation media consisting of RPMI supplemented with 2 mg/ml collagenase I, 5% FBS and 15 U/ml DNAse. Samples were dissociated using the gentleMACS dissociator (Miltenyi Biotec), and filtered through a 70 µm cell strainer. After red blood cell lysis, cell suspensions were washed and used as described below.

Flow cytometry and cell sorting

For immune cells analysis of NT2.5 tumors, dissociated cell suspensions were cryopreserved with 90% FBS and 10% DMSO. Once thawed, $5X10^6$ cells per mL were washed with cold PBS and blocked in PBS with Rat Anti-Mouse CD16/CD32 (Mouse BD Fc Block™, BD Biosciences) for 15 min at 4ºC in the dark. Then, staining of cell surface markers for myeloid cell phenotyping was performed by incubating cells with fluorescent-labeled primary antibodies for 30 min at 4 ºC in the dark. Cells were then fixed and permeabilized using Cyto-Fast™ Fix/Perm Buffer Set (Biolegend) before intracellular staining of Arginase I. LIVE/DEAD™ Fixable Aqua Dead Cell Stain Kit (ThermoFisher) was used as a viability marker. Antibodies used were CD86 (Biolegend, 105037), F4/80 (Biolegend 123141), MHCII (BD Biosciences 562009), Ly6C (Biolegend, 128012), CD11b (Biolegend, 101207), CD206 (Biolegend, 141732), Ly6G (BD Biosciences, 560599), CD11c (BD Biosciences, 560583), CD3 (BD Biosciences,

560590) and Arginase 1 (Thermo Fisher 48-3697-82). For MHC-I analysis, BRx68 cells grown in different conditions were stained with HLA-ABC antibody (Biolegend, 311410). The myeloid-derived suppressor cells (MDSC) were gated by $CD3^-/CD11^+/MHCII^-$ and macrophages were gated by $CD3^-/MHCII^+/F4/80^+$. The granulocytic MDSCs (gMDSCs) were identified as $Ly6G^+/Ly6C^{int}$ MDSCs and myeloid MDSCs (mMDSCs) were identified as $Ly6G^{low}/Ly6C^+$ MDSC. The Attune NxT cyometer (Thermo Fisher Scientific) was used for these analyses.

For FACS sorting, cell suspensions from MCF7-HypT tumors were washed with PBS, blocked in PBS with 10% FBS and 1 µg/ml mouse Fc Block (BD Biosciences) for 15 minutes and incubated with the human-specific anti-CD298-APC antibody (Biolegend, 341706) for 30 minutes. DAPI (1 µg/ml) was used as a viability marker. $CD298^+DAPI^-GFP^+RFP^-$ and $CD298^+DAPI^-GFP^-RFP^+$ cells were sorted into pre-chilled tubes with PBS, centrifuged and lysed with Quick RNA lysis buffer to proceed with RNA extraction. For sorting RFP+ cells from MCF7-HypT cells grown *in vitro*, cells were collected, resuspended in cold 1% BSA in PBS with DAPI (1 µg/ml), and sorted. FACS Aria II (BD Biosciences) was used for cell sorting.

Single cell RNAseq

The Chromium™ Single Cell Reagent Kit v2 (10x Genomics) was used for single cell RNAseq. Tumors from 12- and 16-week-old mice were dissociated as previously described. After washes with cold PBS with 0.04% BSA, 6000 cells were loaded into a Single Cell A Chip. Library preparation was done following manufacturer's instructions. Libraries were sequenced on NextSeq (Illumina). The raw fastq files were processed with Cell Ranger 3.0.2 from 10x Genomics to generate a sparse matrix of features by barcodes. This output was then loaded into

R version 4.0.2 and processed with the R package Seurat 4.0.0(Satija et al., 2015). The data was then filtered with standard quality control to remove cells with few genes expressed or an overrepresentation of mitochondrial reads. Data was then scaled and normalized. Linear reduction analysis was performed by calculation of PCA from the most variable genes. Cells were then clustered using a resolution of 0.5 and visualized by UMAP. Marker genes were used to identify different cell types present. IFN/AP and Hypoxia scores were generated using the AddModuleScore function, with a control value of 5. Tumor cells were binned into deciles by IFN/AP score, and Hypoxia score was then plotted for each decile with the DotPlot function.

Fluorescent immunohistochemistry

Primary tumors and lungs were fixed in 4% PFA for 4.5 hours, washed three times with cold PBS and cryoprotected in PBS with 30% sucrose at 4ºC overnight. Tissues were then embedded in OCT, frozen using dry ice/ethanol baths and stored at -80ºC. Cryosections were incubated at 4ºC overnight with antibodies against GFP (Abcam, ab13970), RFP (Abcam, ab62341), pimonidazole (Hypoxyprobe, Pab2627), and CRE (Millipore, mab3120). The secondary antibodies used in this study were Goat anti-Chicken IgY Alexa Fluor 488 (Life Technologies, A11039), Goat anti-Rabbit IgG Alexa Fluor 594 (Life Technologies, A11012) and Goat anti-mouse IgG Alexa Fluor 647 (Life Technologies, A21240). All secondary antibodies were incubated for one hour at room temperature. Images were taken on a Keyence BZ-9000 or an Axioimager A1 (Zeiss) fluorescence microscope.

Gene expression profiling

Integrity of RNA extracted with Quick-RNA MicroPrep (Zymo) was measured using Bioanalyzer (Agilent). Sequencing libraries were prepared with KAPA stranded RNA-Seq Kit with RiboErase (Kapa Biosystems) according to manufacturer's instructions, and single-end 75 bp sequencing was performed at the USC Molecular Genomics Core, using a NextSeq high output 75 cycle kit (Illumina). Reads were trimmed for Nextera and Illumina adapter sequences using trimgalore([CSL STYLE ERROR: reference with no printed form.]) with default parameters. Trimmed reads were mapped to hg19 (GRCh37) reference using STAR (v2.7.1a)(Dobin et al., 2013), and the reads mapped to the genes annotated in the ENSEMBL GRCh37.p13 GTF (release 75) were quantified using HTSeq-count (v0.11.2)(Anders et al., 2015). Differentially expressed genes across hypoxia-normoxia conditions were identified after controlling for cell line and batch effects (FDR≤0.05), using DESeq2 (v1.26.0)(Love et al., 2014). PCA and heatmaps were generated using variance stabilizing transformed normalized counts after regressing out the batch effects using removeBatchEffect function from limma package (v3.42.2)(Ritchie et al., 2015). Pathway analysis was performed using Ingenuity Pathway Analysis (QIAGEN, https://www.qiagenbioinformatics.com/products/ingenuitypathway-analysis) and overlapping gene sets were found using Gene Set Enrichment Analysis at https://www.gsea-msigdb.org/gsea(Mootha et al., 2003; Subramanian et al., 2005).

RNA-Seq data of different breast cancer cell lines were obtained from Gene Expression Omnibus (GEO). Genes differentially expressed in responder cell lines (MCF7, T47D, and BT4774) compared to non-responder cell lines (231 and HS578T) were identified using DESeq2 after controlling for cell lines differences and study specific difference at their respective GSE level. Microarray expression data of mouse Py117 and Py8119 cancer cells were

obtained from (GSE118181)(Aguilera et al., 2020). Differentially expressed (DE) genes between responsive and non-responsive clones were identified using limma(Ritchie et al., 2015) at an FDR level of 0.05. After mapping RefSeq IDs to ENSEMBL IDs, common orthologous DE genes in responder RNA-seq breast cancer cell lines and mouse Py117 were identified from the two analysis.

Chromatin accessibility assay and motif identification

ATAC-seq was performed as previously described(Buenrostro et al., 2015). In brief, nuclei of 50,000 cells per sample were extracted using a non-ionic lysis buffer (10mM Tris pH 7.4, 10 mM NaCl, 3 mM $MgCl_2$, 0.1% (v/v Igepal CA630). After incubating the nuclei with Tn5 transposase for 30 minutes at 37ºC, libraries were generated and purified using Agencourt AMPure XP beads (Beckman Coulter). Library quality was assessed using a Bioanalyzer high-sensitivity DNA analysis kit (Agilent), and paired-end 75 bp sequencing was performed using a NextSeq 500/500 150 cycle kit (Illumina) at the USC Molecular Genomics Core. After adapter trimming with trimgalore([CSL STYLE ERROR: reference with no printed form.]), reads were mapped to hg19 reference using Bowtie 2 (v2.2.8)(Langmead and Salzberg, 2012) with parameters -X 2000 –fr –no-discordant –no-mixed –minins 38. Only non-mitochondrial reads with a minimum mapping quality score (≤30) were kept for the downstream analysis. Duplicate reads were removed using Picard (v2.23.4). All mapped reads were offset by +4 bp for the + strand and -5 bp for the - strand(Buenrostro et al., 2015). Peaks were identified for each sample using MACS2 (v2.2.7.1)(Zhang et al., 2008) with parameters -q 0.01 –shift -100 –extsize 200 –nomodel –nolambda. Peaks intersecting with the ENCODE blacklisted regions were removed. For differential analysis, overlapping peaks across conditions were merged using BEDtools

(v2.29.2)(Quinlan and Hall, 2010) to obtain a union set and reads aligning to this set were counted using featureCounts (v2.0.0)(Liao et al., 2014). Differentially accessible peaks were then identified from this union set using DESeq2(Love et al., 2014). All analyses and plots were generated using R.

Motif enrichment was performed using top 1K differentially open regions (foreground sequences) with respect to three different background sequences: top 1K differentially closed regions, flanking sequences of identical length and randomly shuffled foreground sequences. To have identical length distribution, both the foreground and background sequences were resized around the center to have the median length of the top 1K foreground sequences. *motifclass* module of cread2(Smith et al., 2006) was used to identify the enrichment of known motifs using a custom TRANSFAC position frequency matrix including JASPAR database(Jolma et al., 2013; Sandelin et al., 2004) and manually curated motifs.

qRT-PCR

Total RNA extracted with Quick-RNA MicroPrep (Zymo) was reverse transcribed using iScript Reverse Transcription Supermix (Bio-Rad), according to the manufacturer's instructions. Real time PCR was performed on a CFX96™ Real-Time PCR detection system (Bio-Rad), using iTaq™ Universal SYBR® Green Supermix (Bio-Rad). The primer sequences used were human IFIT1 (forward, 5'-AGAAGCAGGCAATCACAGAAAA-3'; reverse, 5'-CTGAAACCGACCATAGTGGAAAT-3'); human IFIT3 (forward, 5'-'AGGCTCTGGAAGAAAAGCCC-3', reverse, 5'-TTCTGCAGTTTCAGGCCCAA-3'); human ISG15 (forward, 5-'GTACAGGAGCTTGTGCCGTG-3'; reverse, 5'-

ACACCTGGAATTCGTTGCCC-3'); human OAS1 (forward, 5'-TGTCCAAGGTGGTAAAGGGTG-3'; reverse, 5'-CCGGCGATTTAACTGATCCTG-3' human CA9 (forward, 5'-GGGTGTCATCTGGACTGTGTT-3'; reverse, 5'-CTTCTGTGCTGCCTTCTCATC-3'); human PHD3 (forward, 5'-GGCTGGGCAAATACTACGTCAA-3'; reverse, 5'-CCTGTTCCATTTCCCGGATAG-3'); human NDRG1 (forward, 5'-GTCCTTATCAACGTGAACCCTT-3'; reverse, 5'-GCATTGGTCGCTCAATCTCCA-3'); human ESR1 (forward, 5'-GTGGGATACGAAAAGACCGA-3'; reverse, 5'-AAGGTTGGCAGCTCTCATGT-3'); human PS2 (forward, 5'- TCGGGGTCGCCTTTGGAGCAG-3'; reverse, 5'-GAGGGCGTGACACCAGGAAAACCA-3'); human 36B4 (forward, 5'-GTGTTCGACAATGGCAGCAT-3'; reverse, 5'-AGACACTGGCAACATTGCGGA-3'); mouse ifit1 (forward, 5'-TCTGCTCTGCTGAAAACCCAG-3'; reverse, 5'-CAAGGAACTGGACCTGCTCTG-3'); mouse isg15 (forward, 5'-GAGCTAGAGCCTGCAGCAAT-3'; reverse, 5'-TCACGGACACCAGGAAATCG-3'); mouse ca9 (forward, 5'-TCTGAAGACAGGATGGAGGAGT-3'; reverse, 5'-AGAGTAGGGTGCCTCCATAG-3'); mouse phd3 (forward, 5'-GGGACAGGTTATGTTCGCCA-3'; reverse, 5'-TGCGGTCTGACCAGAAGAAC-3'); mouse 36B4 (forward, 5'-CTCGTTGGAGTGACATCGTCT-3'; reverse, 5'-GTCTGCTCCCACAATGAAGC-3'). The relative RNA levels were calculated using the DDCq method, using 36B4 as reference gene.

Western blotting

Cells were washed with PBS and lysed in Laemmli buffer (50 mM Tris, pH6.8, 1.25% sodium dodecyl sulfate, 15% glycerol). Cell lysates were heated at 95ºC for 15 minutes for complete lysis and denaturalization, after which proteins were quantified by Lowry protein assay (Bio-Rad) and 5% (v/v) β-mercaptoethanol (Sigma) and 0.004% (w/v) bromophenol-blue (Sigma) were added. Proteins were run on 4-15% SDS-polyacrylamide gradient gels (Bio-Rad) and transferred to a low-fluorescence PVDF membrane (Millipore). Primary antibodies used in this study are HIF1α (BD Biosciences, 610958), HIF2α (R&D, AF2886), ARNT (Cell Signaling, 5537), H3 (Abcam, ab1791), H3K4me3, (Epigentek, A-4033), H3K9me2 (Abcam, ab1220), H3K9me3 (Epigentek, A-4036), H3K27me3 (Millipore, 07-449), H3K36me3 (Epigentek, A4042), H3K27ac (Active Motif, 39133), IRF3 (Cell Signaling, 10949), FOXO1 (Cell Signaling, 2880), FOXA1 (Abcam, ab23738), FOXO3a (Cell Signaling, 2497), and β-actin (Sigma, A5441). Membranes were probed at 4ºC overnight, followed by incubation with an IRDye®-conjugated anti-mouse (LI-COR, 926-32210), anti-rabbit (LI-COR, 926-68071) or anti-goat secondary (LI-COR, 926-32214) antibodies and images were acquired with a LI-COR Odyssey CLx Near-Infrared Fluorescence Imaging System. Alternatively, anti-mouse-HRP (BioRad, 1706516) or anti-rabbit-HRP (Jackson Labs, 711035152) antibodies were used.

Statistical analysis

Results represent mean±SEM, unless otherwise indicated. Statistical significance between two groups was determined by unpaired Student's t-test or Mann-Whitney test, or ANOVA for more than 2 groups followed by Fisher's LSD test. Statistical analysis was done with GraphPad Prism v.9.

FIGURE 1

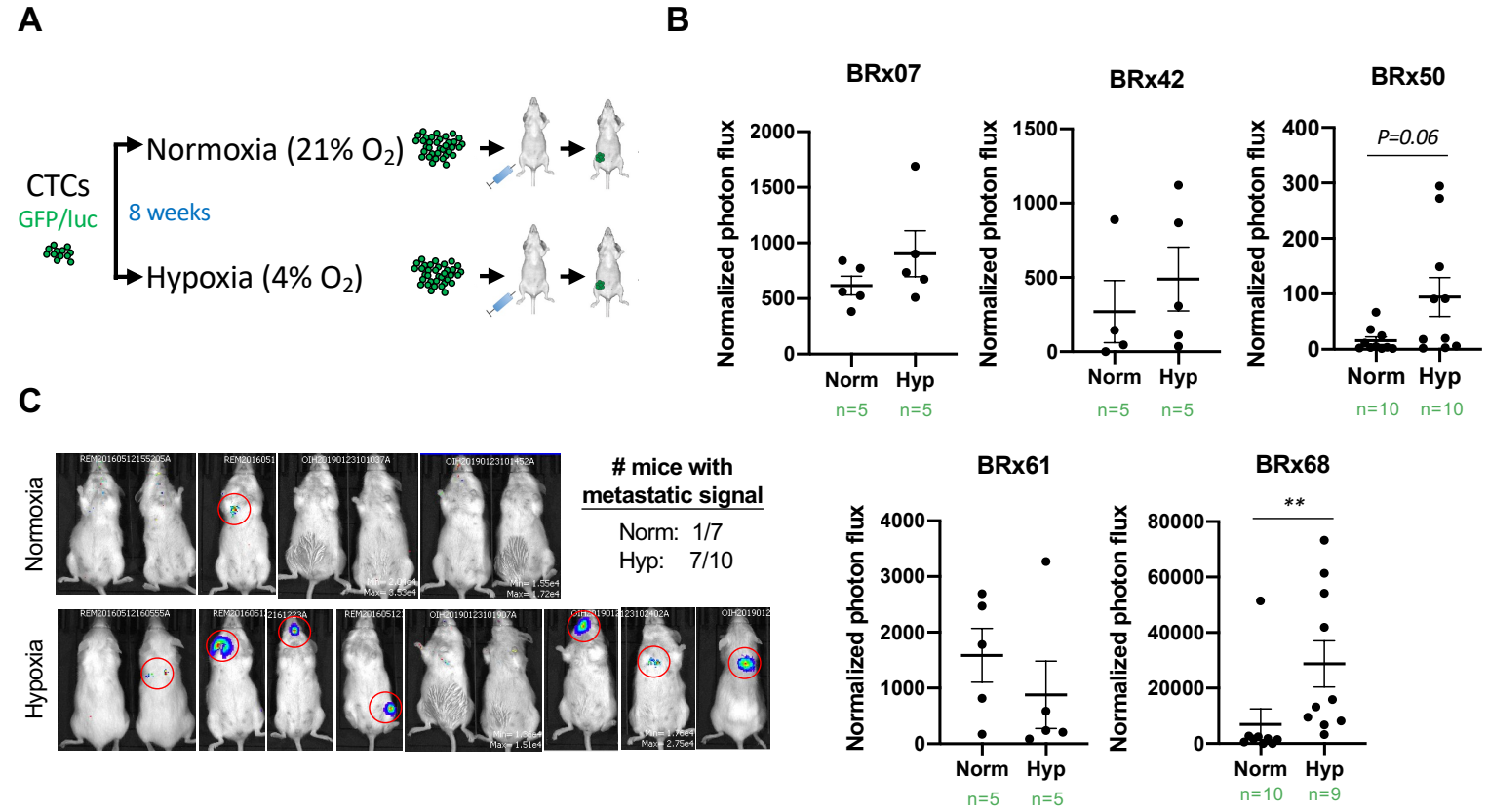
A
CTCs
GFP/luc
8 weeks
Normoxia (21% O2)
Hypoxia (4% O2)
B
BRx07
BRx42
BRx50
Normalized photon flux
P=0.06
Norm
Hyp
n=5
n=10
C
Normoxia
Hypoxia
mice with metastatic signal
Norm: 1/7
Hyp: 7/10
BRx61
BRx68
**
n=9

Figure 1: Hypoxia promotes primary tumor growth and metastasis formation in certain breast cancer CTC lines.

(A) Schematic representation of xenotransplantation experiments. Cells constitutively expressing GFP and luciferase (GFP/luc) were grown in normoxia or hypoxia for 8 weeks and injected into the 4th mammary fat pads or tail veins of NSG mice. **(B)** Tumor growth in mice orthotopically injected with different CTC lines (2,000 cells per mouse for BRx07, BRx61 and BRx68, 20,000 cells per mouse for BRx42 and BRx50), measured by bioluminescence. Normalized photon flux at 12 weeks after injection. Means ±SEM are shown. n = number of mice. P values were obtained with 2-tailed Mann-Whitney test. *P<0.05, **P<0.01. **(C)** Bioluminescence imaging data of mice 14 weeks after intravenous injection of 100,000 BRx68-GFP/luc cells per mouse.

FIGURE 2

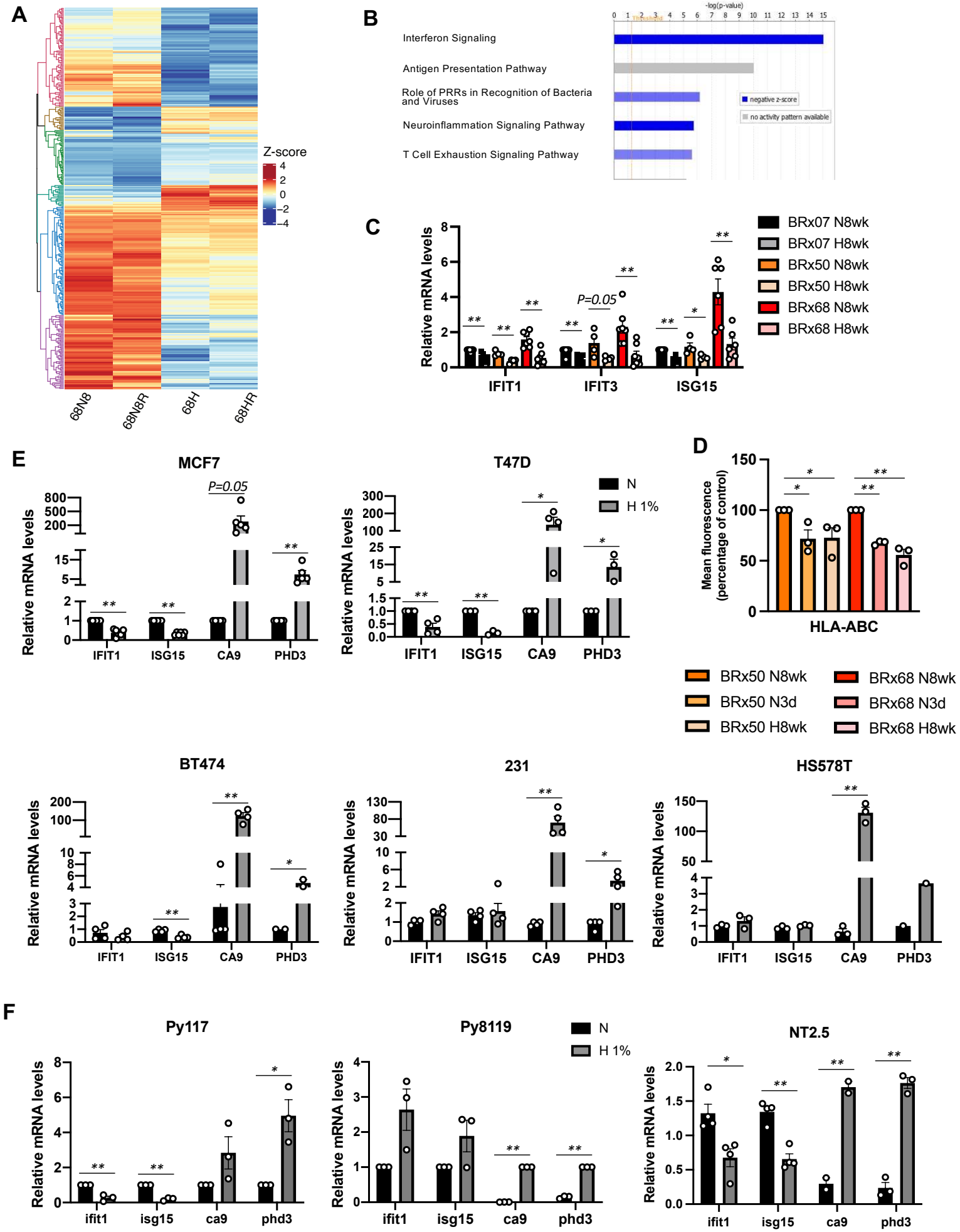
A
Z-score
4
2
0
−2
−4
68N8
68N8R
68H
68HR
B
-log(p-value)
Threshold
Interferon Signaling
Antigen Presentation Pathway
Role of PRRs in Recognition of Bacteria and Viruses
Neuroinflammation Signaling Pathway
T Cell Exhaustion Signaling Pathway
negative z-score
no activity pattern available
C
Relative mRNA levels
P=0.05
IFIT1
IFIT3
ISG15
BRx07 N8wk
BRx07 H8wk
BRx50 N8wk
BRx50 H8wk
BRx68 N8wk
BRx68 H8wk
E
MCF7
T47D
N
H 1%
Relative mRNA levels
P=0.05
IFIT1
ISG15
CA9
PHD3
D
Mean fluorescence (percentage of control)
HLA-ABC
BRx50 N8wk
BRx50 N3d
BRx50 H8wk
BRx68 N8wk
BRx68 N3d
BRx68 H8wk
BT474
231
HS578T
Relative mRNA levels
IFIT1
ISG15
CA9
PHD3
F
Py117
Py8119
NT2.5
N
H 1%
Relative mRNA levels
ifit1
isg15
ca9
phd3

Figure 2: Hypoxia downregulates type I IFN and AP pathways in luminal breast cancer cells. **(A)** Heatmap depicting genes differentially expressed in BRx68 cells grown in normoxia (N) or hypoxia (H, 4% O_2) for 8 weeks. **(B)** Top canonical pathways enriched in genes differentially expressed in BRx68 cells cultured in normoxia or hypoxia (4% O_2). Graph shows -log(p-value). Blue bar indicates negative z-score. **(C)** qPCR analysis of 3 IFN target genes in CTC lines grown in normoxia or hypoxia (4% O_2) for 8 weeks. Means ±SEM of 7 (BRx07 and BRx68) or 4 (BRx50) experiments are shown. P value was calculated with 2-tailed Student's *t* test. *P<0.05, **P<0.01. **(D)** Flow cytometry analysis of relative level of HLA-ABC in BRx68 and BRx50 cells cultured for 8 weeks in normoxia (N8), 3 days in normoxia (N3), and 8 weeks in hypoxia (H8). Means ±SEM, n=3, P value was calculated with one-way ANOVA followed by Fisher's LSD test. *P<0.05, **P<0.01. **(E-F)** qPCR analysis of 2 IFN target genes (IFIT1, ISG15) and 2 HIF target genes (CA9, PHD3) in different breast cancer cell lines of human **(E)** or mouse **(F)** origin cultured in normoxia or hypoxia (1% O_2) for 3 days. Means ±SEM. P values were calculated with 2-tailed Student's *t* test * p<0.05, ** p<0.01.

FIGURE 3

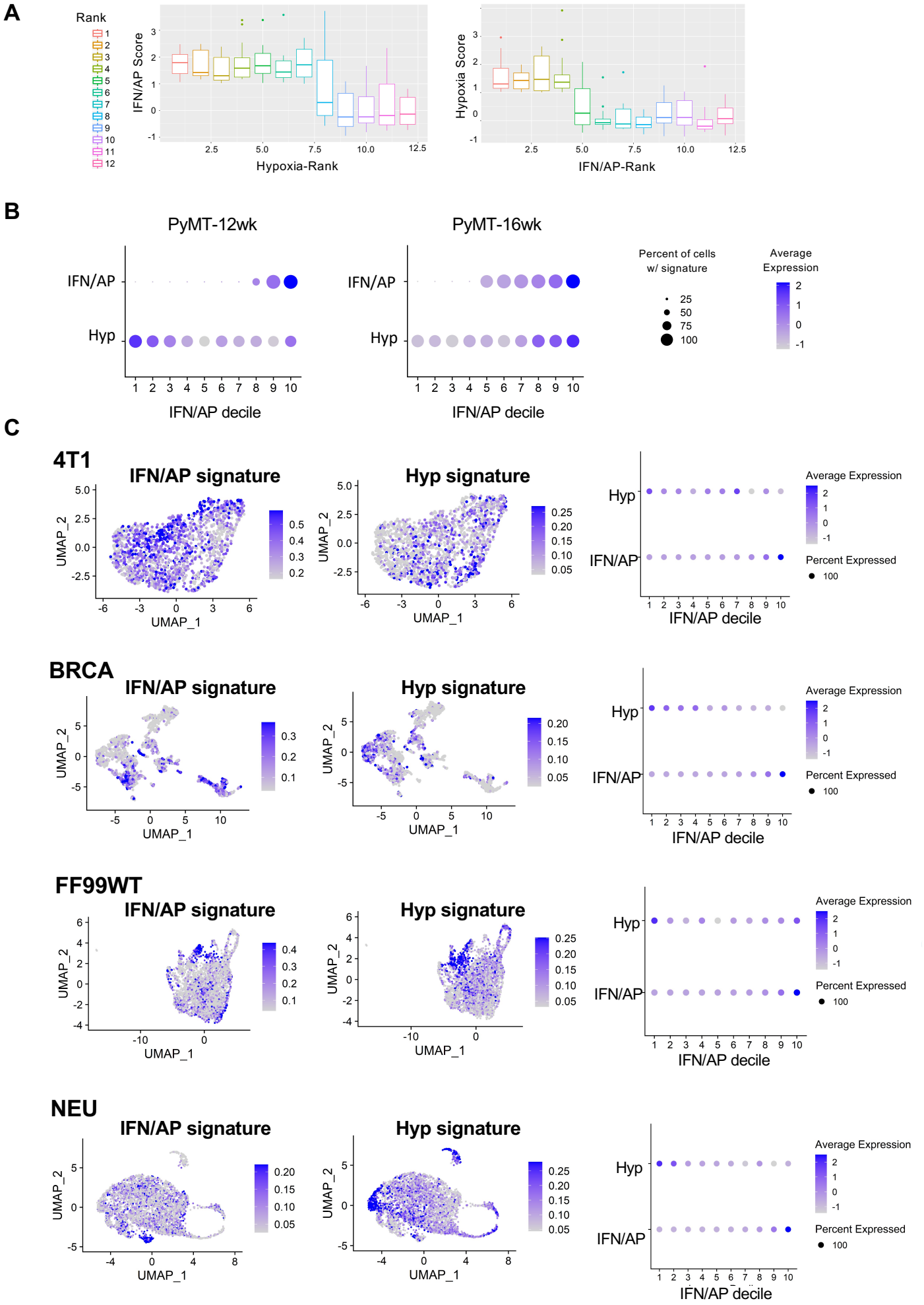
A
Rank
IFN/AP Score
Hypoxia-Rank
Hypoxia Score
IFN/AP-Rank
B
PyMT-12wk
PyMT-16wk
IFN/AP
Hyp
IFN/AP decile
Percent of cells w/ signature
Average Expression
C
4T1
BRCA
FF99WT
NEU
IFN/AP signature
Hyp signature
UMAP_1
UMAP_2
Percent Expressed

Figure 3: Inverse correlation of hypoxia and IFN/AP signatures in *in vivo* breast tumors and tumor cells of mouse mammary tumors.

(A) Graph illustrating inverse correlation between hypoxia signature and IFN/AP signature in breast tumors from TCGA. Tumors with detectable scores of hypoxia signature or IFN/AP signature based on RNA-seq analysis were plotted according to the hypoxia score rank (X-axis, Hypoxia-Rank) and IFN/AP Score (Y-axis) or vice versa. **(B)** Decile maps of tumor cell population based on hypoxia and IFN/AP scores for MMTV-PyMT tumors at 12 weeks or 16 weeks. Cell deciles were ranked by IFN/AP scores. **(C)** UMAP plots (left) and decile maps (right) of tumor cell population based on IFN/AP and hypoxia scores for murine breast cancer syngeneic models. Cell deciles were ranked by IFN/AP scores.

FIGURE 4

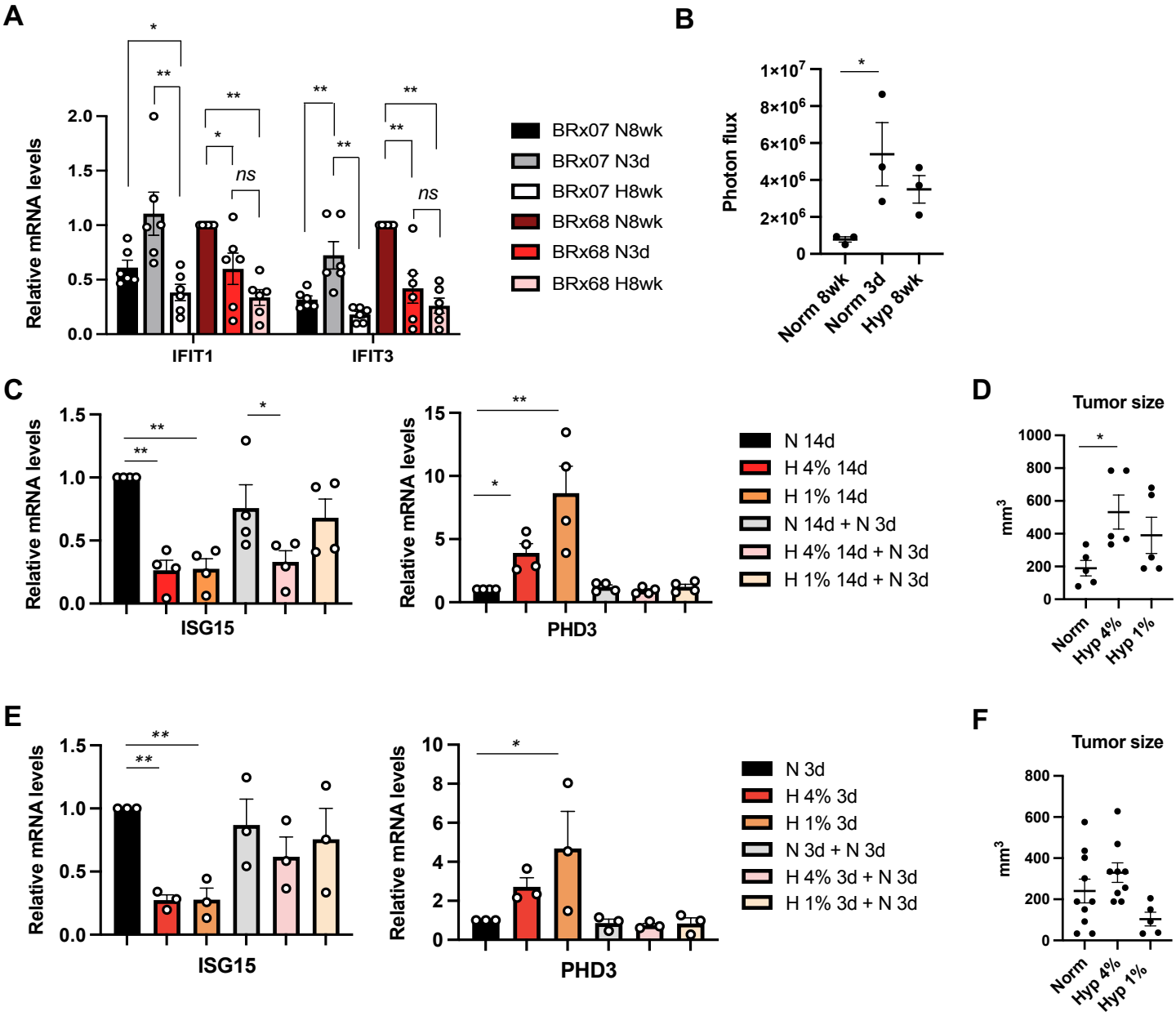
A
Relative mRNA levels
IFIT1
IFIT3
ns
BRx07 N8wk
BRx07 N3d
BRx07 H8wk
BRx68 N8wk
BRx68 N3d
BRx68 H8wk
B
Photon flux
Norm 8wk
Norm 3d
Hyp 8wk
C
ISG15
PHD3
N 14d
H 4% 14d
H 1% 14d
N 14d + N 3d
H 4% 14d + N 3d
H 1% 14d + N 3d
D
Tumor size
mm3
Norm
Hyp 4%
Hyp 1%
E
ISG15
PHD3
N 3d
H 4% 3d
H 1% 3d
N 3d + N 3d
H 4% 3d + N 3d
H 1% 3d + N 3d
F
Tumor size
mm3
Norm
Hyp 4%
Hyp 1%

Figure 4: Hypoxic memory of type I IFN suppression is associated with enhanced tumorigenesis and metastasis.

(A) Relative mRNA expression levels of IFIT1 and IFIT3 in BRx07 and BRx68 cells grown in hypoxia for 8 weeks (4% O_2, H8), or in normoxia for 8 weeks (N8) or 3 days (N3). Means ±SEM, n=6, P value was obtained with one-way ANOVA followed by Fisher's LSD test. *P<0.05, ** P<0.01. **(B)** Bioluminescence values from primary tumors 6 weeks after orthotopic injection of 2,000 BRx68-GFP/luc cells. Prior to injection, cells were grown in hypoxia (4% O_2) for 8 weeks, normoxia for 8 weeks, or normoxia for 3 days. Means ±SEM, n=3. P values were calculated with one-way ANOVA followed by Fisher's LSD test. *P<0.05. **(C)** qPCR analysis of relative mRNA expression levels of the IFN target ISG15 and the hypoxia target PHD3 in MCF7 cells grown in normoxia or hypoxia (4% O_2 or 1% O_2) for 14 days followed by an additional 3 days of reoxygenation. Means ±SEM, n=4. P values were obtained with one-way ANOVA followed by Fisher's LSD test. *P<0.05, ** P<0.01. **(D)** Tumor volumes formed by MCF7 cells cultured in normoxia or hypoxia (4% or 1%) for 14 days. Means ±SEM, n=5, P values were obtained with one-way ANOVA followed by Fisher's LSD test. *P<0.05. **(E)** qPCR analysis of relative mRNA expression levels of the IFN target ISG15 and the hypoxia target PHD3 in MCF7 cells grown in normoxia or hypoxia (4% O_2 or 1% O_2) for 14 days followed by an additional 3 days of reoxygenation. Means ±SEM, n=4. P values were obtained with one-way ANOVA followed by Fisher's LSD test. *P<0.05, ** P<0.01. **(F)** Tumor volumes formed by MCF7 cells cultured in normoxia or hypoxia (4% or 1%) for 14 days. Means ±SEM, n=5, P values were obtained with one-way ANOVA followed by Fisher's LSD test. *P<0.05.

FIGURE 5

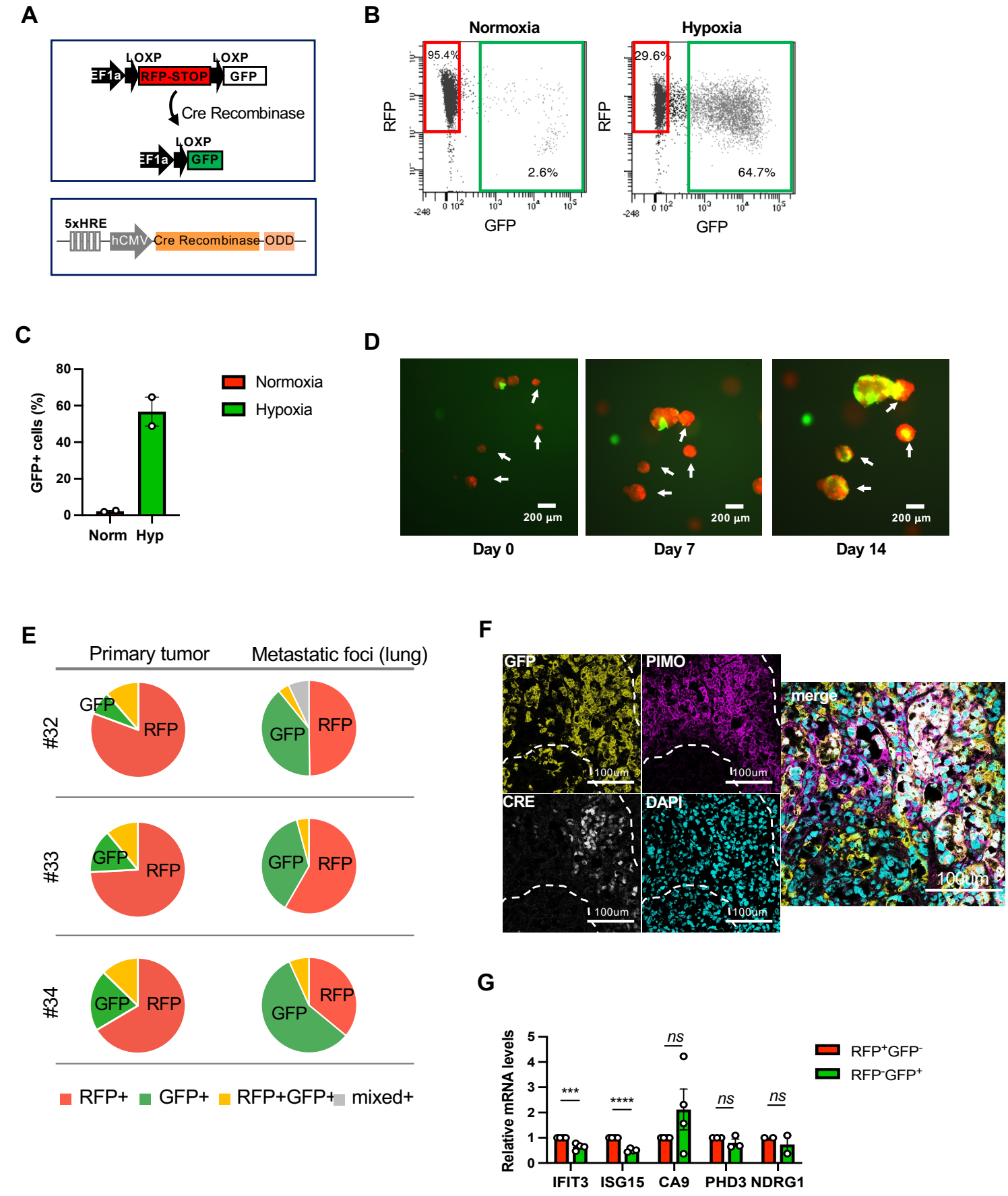
A
LOXP
LOXP
EF1a
RFP-STOP
GFP
Cre Recombinase
LOXP
EF1a
GFP
5xHRE
hCMV
Cre Recombinase
ODD
B
Normoxia
Hypoxia
95.4%
2.6%
29.6%
64.7%
RFP
GFP
C
GFP+ cells (%)
80
60
40
20
0
Norm
Hyp
Normoxia
Hypoxia
D
200 µm
Day 0
Day 7
Day 14
E
Primary tumor
Metastatic foci (lung)
#32
#33
#34
GFP
RFP
RFP+
GFP+
RFP+GFP+
mixed+
F
GFP
PIMO
merge
CRE
DAPI
100um
G
Relative mRNA levels
***
****
ns
IFIT3
ISG15
CA9
PHD3
NDRG1
RFP+GFP-
RFP-GFP+

Figure 5: Hypoxia-tracing reporter system showed tumor cells with hypoxic memory and enhanced metastatic capacity.

(A) Schematic representation of the plasmids used to create the hypoxia tracing MCF7-HypT cells. **(B-C)** Representative FACS plots **(B)** and bar graph **(C)** showing the percentage of GFP+ cells in MCF7-HypT cells cultured in normoxia or hypoxia (1% O_2) for 3 days. **(D)** Fluorescence microscopy images of MCF7-HypT cells cultured in 3D collagen-Matrigel gels. Arrows point at spheres formed exclusively by RFP-positive cells on the day of starting the 3D culture. Scale bar = 200 mm. **(E)** Quantification of RFP and GFP positive area in primary tumors (left) and metastatic loci in lungs (right). Mouse number is labeled on the left. **(F)** Representative fluorescent images of a MCF7-HypT tumor section stained with antibodies against GFP (green), pimonidazole (white) and Cre (red). Nuclei were stained with DAPI (blue). Dotted line contours the hypoxic region. Scale bars = 100 µm. **(G)** Relative mRNA levels of IFN targets (IFIT3 and ISG15) and hypoxia targets (CA9, PHD3 and NDRG1) in $RFP^{+}GFP^{-}$ and $RFP^{-}GFP^{+}$ cell populations sorted from MCF7-HypT tumors. Means ±SEM, n=4, P values were obtained with 2-tailed Student's t test. *P<0.05, ns: no significance.

FIGURE 6

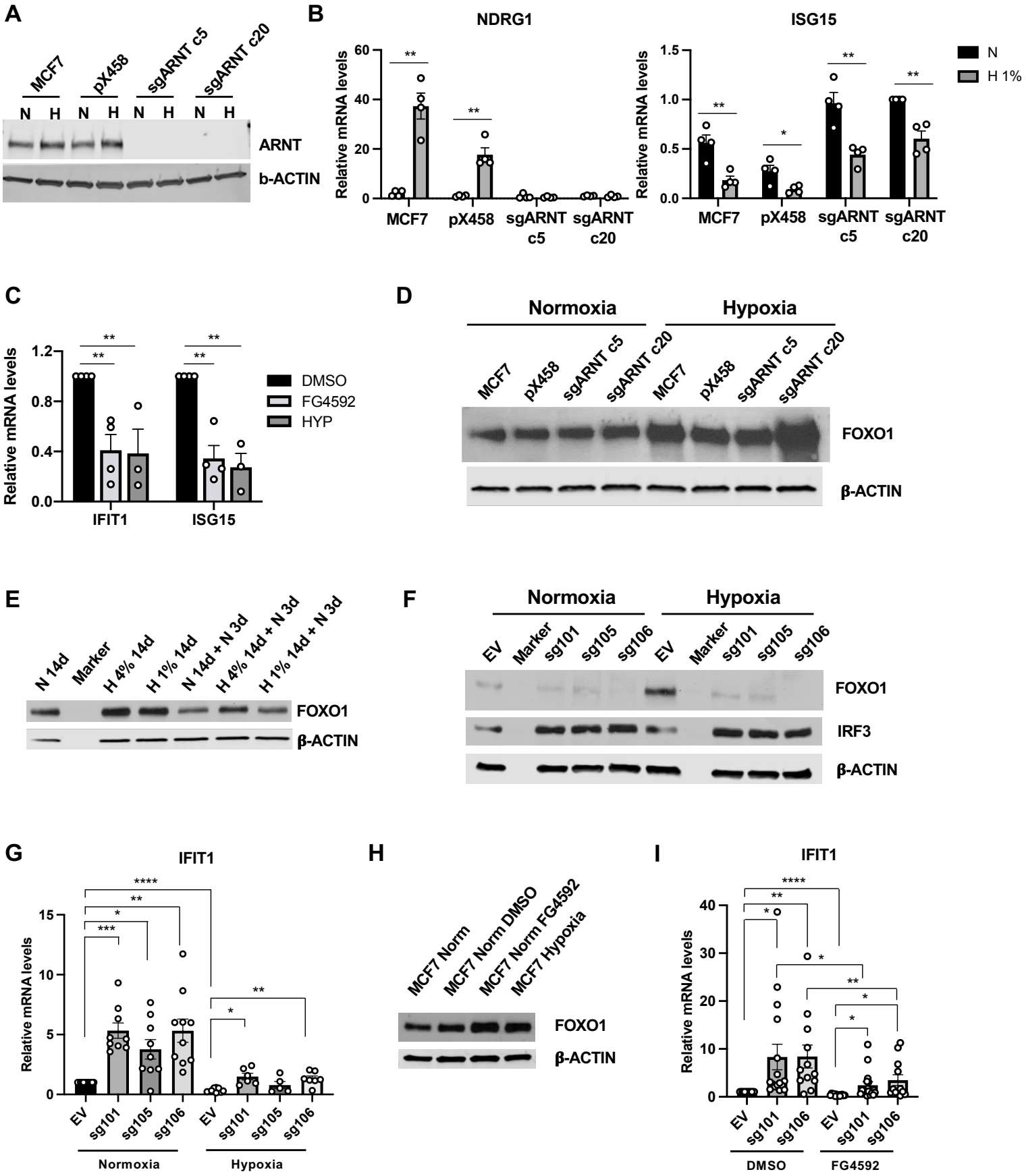
A
MCF7
pX458
sgARNT c5
sgARNT c20
N H N H N H N H
ARNT
b-ACTIN
B
NDRG1
ISG15
Relative mRNA levels
N
H 1%
MCF7
pX458
sgARNT c5
sgARNT c20
C
Relative mRNA levels
DMSO
FG4592
HYP
IFIT1
ISG15
D
Normoxia
Hypoxia
MCF7
pX458
sgARNT c5
sgARNT c20
FOXO1
β-ACTIN
E
N 14d
Marker
H 4% 14d
H 1% 14d
N 14d + N 3d
H 4% 14d + N 3d
H 1% 14d + N 3d
FOXO1
β-ACTIN
F
Normoxia
Hypoxia
EV
Marker
sg101
sg105
sg106
FOXO1
IRF3
β-ACTIN
G
IFIT1
Relative mRNA levels
EV
sg101
sg105
sg106
Normoxia
Hypoxia
H
MCF7 Norm
MCF7 Norm DMSO
MCF7 Norm FG4592
MCF7 Hypoxia
FOXO1
β-ACTIN
I
IFIT1
Relative mRNA levels
EV
sg101
sg106
DMSO
FG4592

Figure 6: Hypoxia upregulates FOXO1 in an HIF-independent manner to suppress type I IFN. **(A)** Immunoblot analysis of ARNT expression in ARNT-KO MCF7 cells, bulk MCF7 and a px458 control MCF7 cells. β-ACTIN is shown as a loading control. **(B)** Relative mRNA expression levels of NDRG1 (left) and ISG15 (right) in bulk MCF7 cells, 1 px458 control MCF7 clone and 2 ARNT-KO MCF7 clones grown in normoxia or hypoxia (1% O_2) for 3 days. Means ±SEM, n=4. P values were obtained with one-way ANOVA followed by Fisher's LSD test. **(C)** IFIT1 and ISG15 expression levels in MCF7 cells treated with the PHD inhibitor FG4592 (100 μM) or hypoxia for 3 days. Means ±SEM, n=4. P values were obtained with one-way ANOVA followed by Fisher's LSD test. *P<0.05, ** P<0.01. **(D)** Immunoblot analysis of FOXO1 level in bulk MCF7 cells, 1 px458 control MCF7 clone and 2 ARNT-KO MCF7 clones grown in normoxia or hypoxia for 3 days. **(E)** Immunoblot analysis of FOXO1 level in MCF7 cells cultured in normoxia (N14d) or 4% or 1% hypoxia (4%H14d, 1%H14d), and those reoxygenated for 3 days after 14 day-long culture in different oxygen conditions (N14d+N3d, 4%H14d+N3d, 1%H14d+N3d). **(F)** Immunoblot analysis of FOXO1 and IRF3 levels in MCF7 cells with EV or 3 different sgRNAs against FOXO1, cultured in normoxia or 4% hypoxia. β-ACTIN is shown as a loading control. **(G)** Relative mRNA expression levels of IFIT1 in MCF7 EV or sgFOXO1 cells cultured in normoxia or 4% hypoxia for 3 days. Means ±SEM. n=11 (EV Norm), n=10 (sg106 Norm), n=9 (sg105 Norm), n=8 (sg101 Norm and EV 4%Hyp), n=7 (sg106 4%Hyp), n=6 (sg101 4%Hyp), and n=5 (sg105 4%H). P values were obtained with one-way ANOVA followed by Fisher's LSD test. *P<0.05, ** P<0.01, **** P<0.001. **(H)** Immunoblot analysis of FOXO1 levels in MCF7 cells, without (DMSO) or with treatment of FG4592, or cultured in 4% hypoxia. β-ACTIN is shown as a loading control. **(I)** qPCR analysis showing relative mRNA expression level of IFIT1 and ISG15 in MCF7 treated with DMSO or FG4592, without (EV) or with suppression of FOXO1 (sgFOXO1). Means ±SEM, EV (n=13), sg101 (n=16), sg106 (n=12), P values were obtained with ANOVA followed by Fisher's LSD test. *P<0.05, ** P<0.01, **** P<0.001.

FIGURE 7

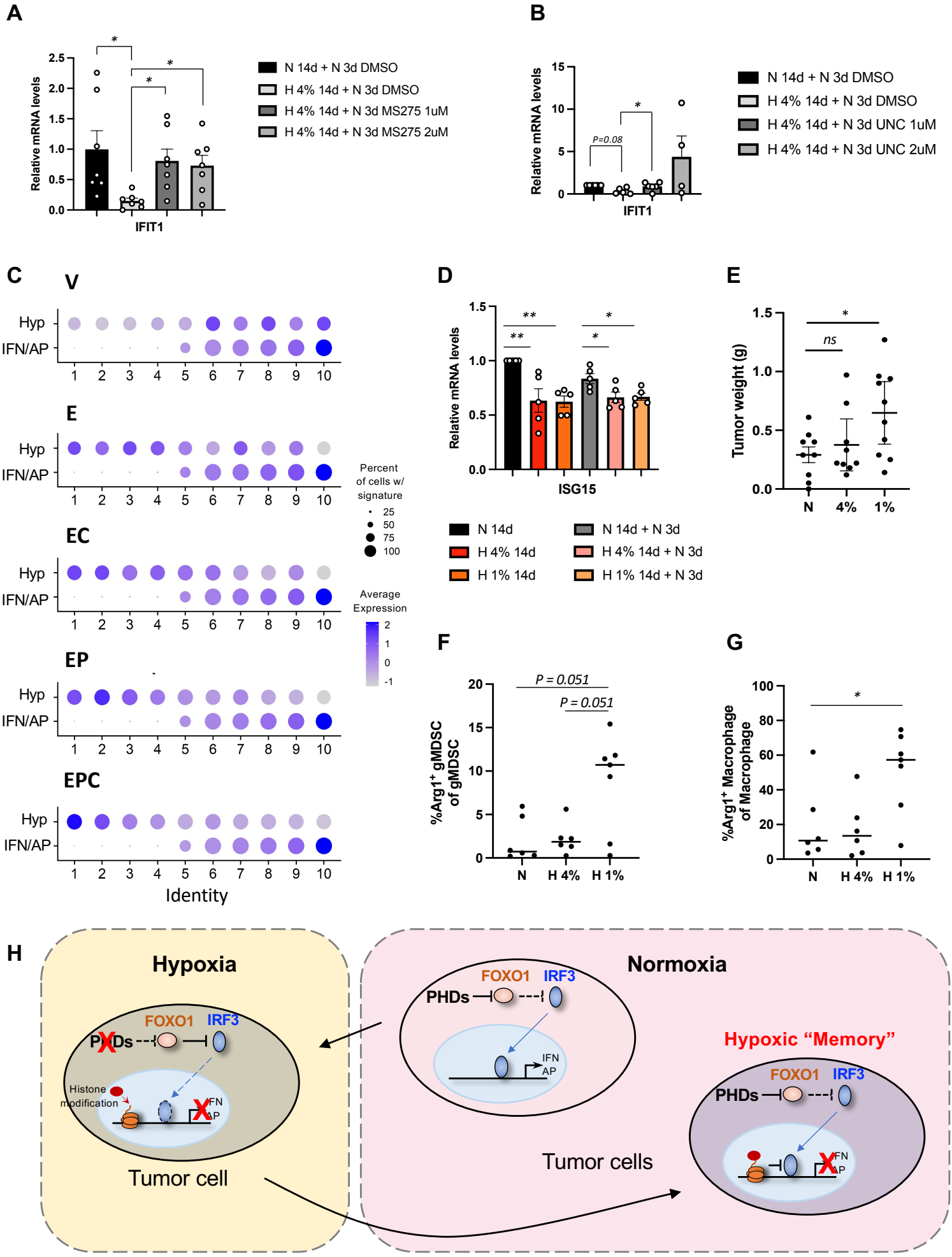
A
Relative mRNA levels
IFIT1
N 14d + N 3d DMSO
H 4% 14d + N 3d DMSO
H 4% 14d + N 3d MS275 1uM
H 4% 14d + N 3d MS275 2uM
B
Relative mRNA levels
P=0.08
IFIT1
N 14d + N 3d DMSO
H 4% 14d + N 3d DMSO
H 4% 14d + N 3d UNC 1uM
H 4% 14d + N 3d UNC 2uM
C
V
E
EC
EP
EPC
Hyp
IFN/AP
Identity
Percent of cells w/ signature
Average Expression
D
Relative mRNA levels
ISG15
N 14d
H 4% 14d
H 1% 14d
N 14d + N 3d
H 4% 14d + N 3d
H 1% 14d + N 3d
E
Tumor weight (g)
ns
N
4%
1%
F
%Arg1+ gMDSC of gMDSC
P = 0.051
P = 0.051
N
H 4%
H 1%
G
%Arg1+ Macrophage of Macrophage
N
H 4%
H 1%
H
Hypoxia
FOXO1
IRF3
PHDs
Histone modification
IFN
AP
Tumor cell
Normoxia
Tumor cells
Hypoxic "Memory"

Figure 7: An HDAC inhibitor can erase hypoxic memory and enhance immune clearance of tumor cells in normoxic regions.

(A-B) Relative mRNA expression levels of IFIT1 in MCF7 cells in reoxygenation experiment (primed in normoxia or hypoxia for 14 days and then reoxygenated in normoxia for 3 days) with or without MS275 **(A)** or UNC0638 **(B)**. n=7, mean±SEM, statistical significance was calculated with Brown-Forsythe and Welch's ANOVA test followed by unpaired t-test with Welch's correction, *p<0.05. **(C)** scRNAseq analysis of hypoxia and IFN/AP scores in tumor cells in the syngeneic mammary tumors formed by NT2.5 cells, treated with vehicle (V), Entinostat (E), Entinostat combined with anti-CTLA4 antibody (EC), with anti-PD1 antibody (EP), or with both (EPC). Decile plot of hypoxia and IFN/AP scores for cell population ranked based on IFN/AP scores. **(D)** Relative mRNA expression levels of isg15 in NT2.5 cells cultured in normoxia, 4% or 1% hypoxia for 14 days, and reoxygenated for 3 days. Means ±SEM, n=5, Statistical significance was calculated with one-way ANOVA followed by Fisher's LSD test. *P<0.05, ** P<0.01. **(E)** Graph showing weight of the orthotopic tumors formed by NT2.5 cells injected into FVB mice at 8 weeks. Means ±SEM. n=9 (Norm), n=9 (Hyp 4%) and n=10 (Hyp 1%). Statistical significance was calculated with one-way ANOVA followed by Fisher's LSD test. *P<0.05. **(F-G)** Graph showing percentage of Arg+ gMDSCs **(F)** and Arg+ macrophages **(G)** in the same tumors formed by NT2.5 cells in (**E**). Statistical significance was calculated with nonparametric Mann-Whitney U test. *P<0.05. **(H)** Graph illustrating a proposed model of hypoxia mediated suppression of IFN/AP and the hypoxic memory.